nature metabolism

ARTICLES

https://doi.org/10.1038/s42255-022-00633-6

Check for updates

Combined alcohol and cannabinoid exposure leads to synergistic toxicity by affecting cerebellar Purkinje cells

Guichang Zou[1,2,7], Jing Xia[1,7], Heyi Luo[1], Dan Xiao[1], Jin Jin[1], Chenjian Miao[1], Xin Zuo[1], Qianqian Gao[3], Zhi Zhang[1], Tian Xue[1], Yezi You[3], Ye Zhang[4], Li Zhang[5] and Wei Xiong[1,2,6] ✉

Combined use of cannabis and alcohol results in greater psychoactive toxicity than either substance alone, but the underlying central mechanisms behind this worsened outcome remain unclear. Here we show that the synergistic effect of Δ⁹-tetrahydrocannabinol (THC) and ethanol on motor incoordination in mice is achieved by activating presynaptic type 1 cannabinoid receptors (CB_1R) and potentiating extrasynaptic glycine receptors (GlyR) within cerebellar Purkinje cells (PCs). The combination of ethanol and THC significantly reduces miniature excitatory postsynaptic current frequency in a CB_1R-dependent manner, while increasing the extrasynaptic GlyR-mediated chronic chloride current, both leading to decreased PC activity. Ethanol enhances THC actions by boosting the blood–brain-barrier permeability of THC and enriching THC in the cell membrane. Di-desoxy-THC, a designed compound that specifically disrupts THC–GlyR interaction without affecting the basic functions of CB_1R and GlyR, is able to restore PC function and motor coordination in mice. Our findings provide potential therapeutic strategies for overcoming the synergistic toxicity caused by combining cannabis and alcohol use.

Psychoactive drugs, such as THC and alcohol, are widely reported to impair motor coordination by targeting the central nervous system (CNS)[1,2]. Notably, cannabis and alcohol have been largely reported to be used in combination, which causes severe motor disorders[3]. Social research studies from various institutions, including the National Highway Traffic Safety Administration of the United States, have warned that combined use of cannabis and alcohol can cause severe motor deficits, leading to compromised traffic safety and increased crashes[4–6]. Animal studies have also shown that systemic ethanol administration significantly enhances THC-induced motor incoordination in mice[7,8]. Although the abnormally enhanced toxicity caused by cannabis and alcohol combination has attracted widespread attention, the mechanism for such synergistic reinforcement remains unclear.

Drug synergism is generally achieved through specific drug targets such as membrane receptors[9]. A large amount of evidence has confirmed that THC and ethanol share several targets on the cell membrane, such as CB_1R and GlyRs[10–17]. The CB_1R is considered one of the most abundant G-protein-coupled receptors in the CNS and it is ubiquitously expressed in the axons and presynaptic terminals of neurons in the CNS[11,12]. GlyR is chloride-permeable pentameric ligand-gated ion channel[17]. Synaptic GlyR mainly mediates inhibitory neurotransmission in the spinal cord and brainstem[18], whereas extrasynaptic GlyR maintains excitability homeostasis in the cerebrum[19,20]. Both CB_1R and GlyR are inextricably linked to motor functions. CB_1R in various brain regions such as the cerebellum, dorsomedial striatum (DMS) and motor cortex (M) is crucial for motor functions such as motor coordination, motor learning and locomotor activity[11,12,21,22]. GlyR dysfunction is also associated with various motor disorders including muscle stiffness, myoclonic jerks, exaggerated startle responses and spasms[23–25].

Although emerging evidence suggests that THC and ethanol can activate or potentiate the function of CB_1R and GlyR[11,12,16,17], whether the two receptors are involved in the synergistic effects of THC and ethanol on motor coordination (SETEM) remains unknown. In this study, we conducted cellular and behavioral experiments using various approaches, including c-Fos immunohistochemistry, electrophysiological recording, chemogenetic manipulations, mass spectrometry, imaging flow cytometry, live animal imaging and behavioral tests, to reveal the molecular and cellular mechanisms underlying the SETEM and develop potential cures.

Results

Cerebellar lobules 4/5 mediate the SETEM. To assess the motor coordination of mice, we constructed an accelerating rotarod (AR) behavioral paradigm[20]. Mice received intraperitoneal (i.p.) administration of various doses of THC and ethanol, either alone or in combination. THC and ethanol both dose-dependently caused motor incoordination, as reflected by reduced latency in the AR test (Extended Data Fig. 1a–d)[26]. Although low-dose THC (i.p. 1.0 mg kg^{-1}) was insufficient to affect AR performance (Extended Data Fig. 1b), the combination of the THC with various doses of ethanol (i.p. 0.5, 1.0 and 2.0 g kg^{-1}) caused more severe motor incoordination than ethanol alone (Fig. 1a,b and Extended Data Fig. 1e–g), suggesting a synergistic effect. Furthermore, such synergistic effect of THC and ethanol showed no differences between male and

[1]Institute on Aging and Brain Disorders, The First Affiliated Hospital of USTC, Division of Life Sciences and Medicine, University of Science and Technology of China, Hefei, China. [2]Institute of Artificial Intelligence, Hefei Comprehensive National Science Center, Hefei, China. [3]CAS Key Laboratory of Soft Matter Chemistry, Department of Polymer Science and Engineering, University of Science and Technology of China, Hefei, China. [4]Department of Anesthesiology and Perioperative Medicine, The Second Hospital of Anhui Medical University, Hefei, China. [5]Laboratory for Integrative Neuroscience, National Institute on Alcohol Abuse and Alcoholism, National Institutes of Health, Bethesda, MD, USA. [6]Anhui Province Key Laboratory of Biomedical Aging Research, Hefei, China. [7]These authors contributed equally: Guichang Zou, Jing Xia. ✉e-mail: wxiong@ustc.edu.cn

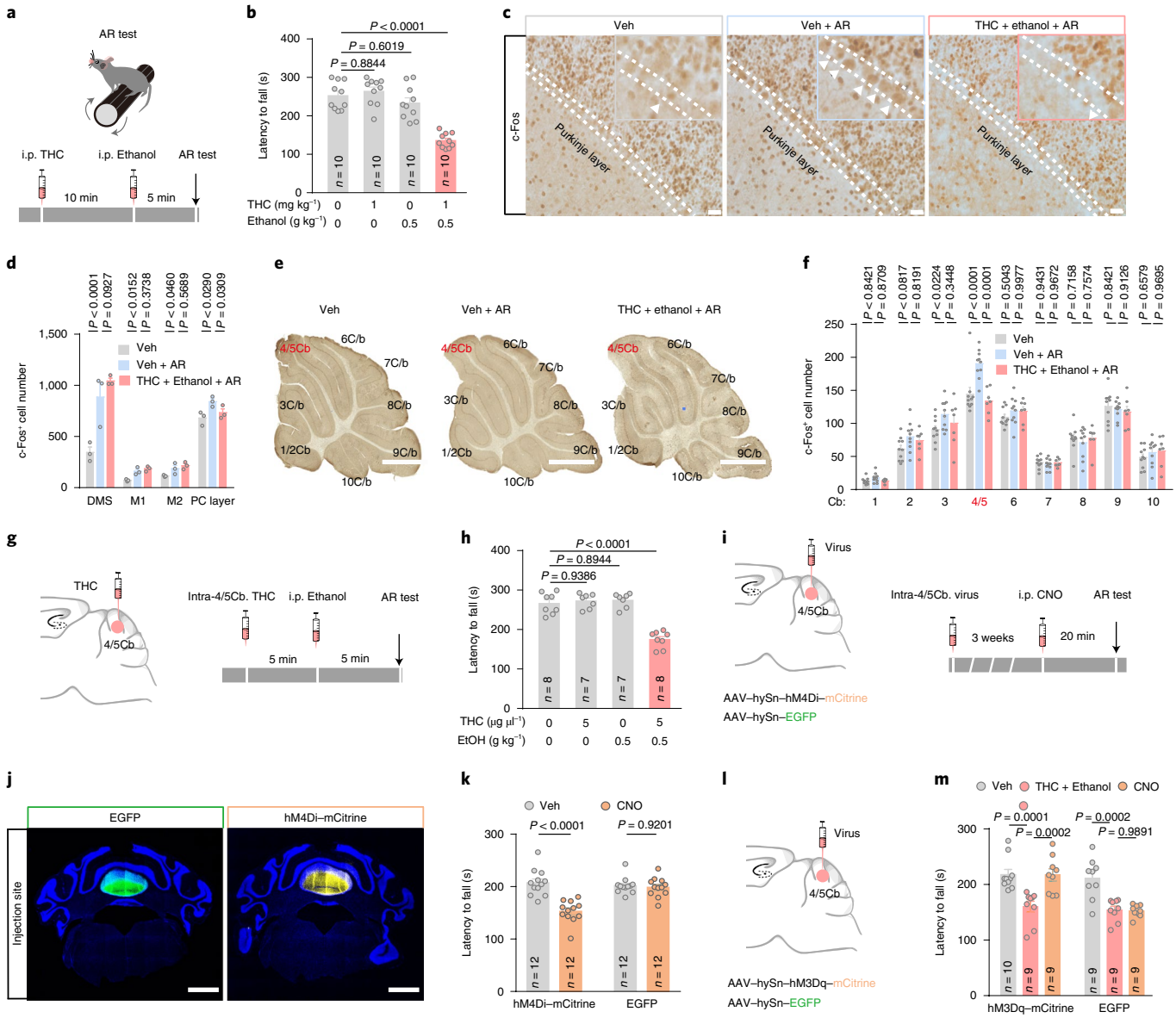

Fig. 1 | Identification of the role of 4/5Cb neurons in the SETEM. a, Schematic showing the timeline of drug administration and AR procedure. **b**, Effects of THC (i.p. 1.0 mg kg^{-1}) and ethanol (i.p. 0.5 g kg^{-1}), either alone or in combination, on AR latency of mice. **c**,**d**, Representative images (**c**) and numbers of c-Fos$^+$ cells (**d**) from immunohistochemistry analysis of c-Fos-positive neurons in various brain regions of mice. Veh, vehicle; M1, motor cortex 1; M2, motor cortex 2. Scale bar, 25 μm. $n = 3$ mice per group. **e**,**f**, Representative images (**e**) and numbers of c-Fos$^+$ cells (**f**) from immunohistochemistry analysis of c-Fos-positive neurons in various cerebellar lobes. Scale bar, 500 μm. $n = 7$–10 mice per group. **g**, Schematic showing the timeline of drug injections and AR procedure. **h**, Effects of THC (intra-4/5Cb, 5 μg μl^{-1}) and ethanol (i.p. 0.5 g kg^{-1}) in combination on the AR latency of mice. **i**, Schematic showing virus injection and timeline of the chemogenetic experimental procedure. **j**, Representative images showing the EGFP or mCitrine signals in the injection sites of the 4/5Cb of mice. Scale bar, 1 mm. **k**, Effects of CNO (i.p. 1.0 mg kg^{-1}) on AR latency of mice. **l**, Schematic showing virus injection and chemogenetic experimental procedure. **m**, Effects of CNO (i.p. 1.0 mg kg^{-1}) on the SETEM caused by THC (i.p. 1.0 mg kg^{-1}) and ethanol (i.p. 0.5 g kg^{-1}) combination in mice. Values are represented as means ± s.e.m., n per group. Exact P values are shown. Statistical differences were determined by a one-way analysis of variance (ANOVA) followed by Tukey's post hoc multiple-comparison test (**b**,**h**) or a two-way ANOVA followed by Tukey's post hoc multiple-comparison test (**d**,**f**,**k**,**m**).

female mice (Extended Data Fig. 1h–l), suggesting that there is no sexual dimorphism of the SETEM. The blood ethanol concentration (BEC) ranged from 33 mg dl^{-1} to 270 mg dl^{-1} at 5–45 min after i.p. administration of 0.5, 1.0 and 2.0 g kg^{-1} ethanol; however, THC administration had no effect on the BEC (Extended Data Fig. 1m–o), suggesting that the synergistic effect may not occur in periphery.

Among all brain regions, the cerebellum, M and DMS are most commonly associated with motor coordination[21,22,27,28]. To reveal the brain regions critical for the SETEM, we examined the expression level of c-Fos, an immediate marker of neuronal activation[29]. Various nuclei including the DMS, anterior cerebellar PC layer, M1 and M2 were activated during the AR test, as reflected by significant increases in c-Fos immunofluorescence signals in these brain nuclei (Fig. 1c,d and Extended Data Fig. 2a–c). Notably, activation of the anterior cerebellar PC layer, but not the DMS or M1/M2, was blocked by combined treatment with i.p. THC and i.p. ethanol (Fig. 1d). c-Fos expression in the anterior cerebellum lobules 1–5 (1–5Cbs) PC layer, but not the 6–10Cb PC layer, was obviously

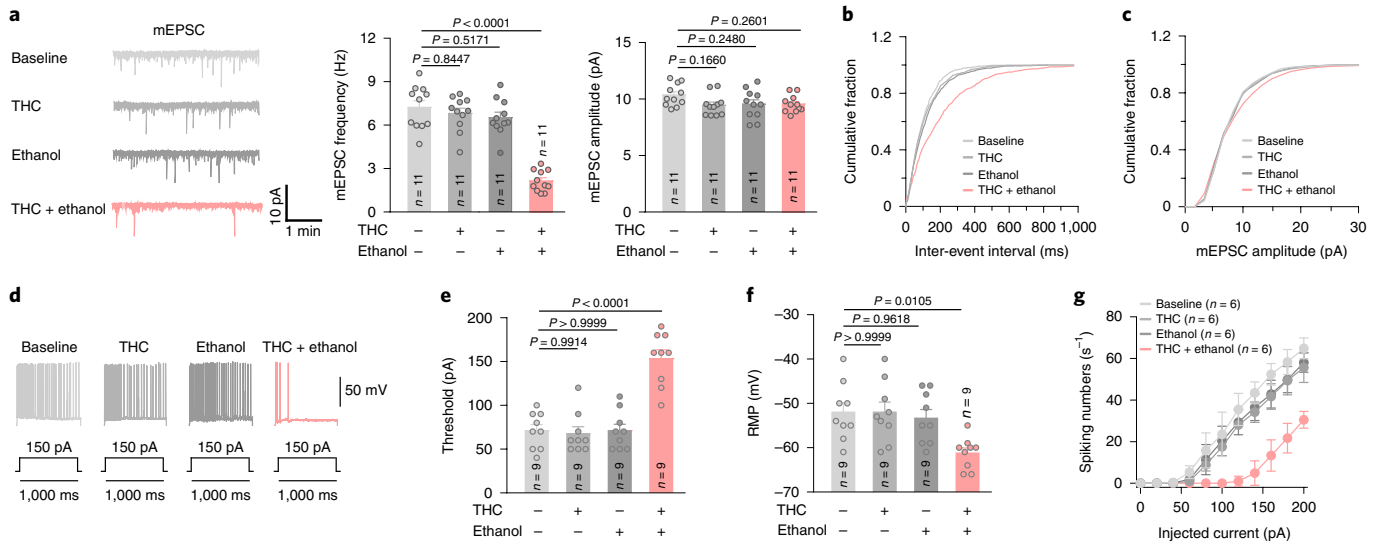

Fig. 2 | Effects of THC and ethanol on PC excitability. a, Trace records, average frequency and amplitude of glutamatergic mEPSCs of PCs in 4/5Cb slices of mice. The brain slices were treated with THC (100 nM, 5 min) and ethanol (20 mM, 5 min), either alone or in combination. **b**,**c**, Cumulative probability plot for the inter-event interval (**b**) and amplitudes (**c**) for glutamatergic mEPSCs of PCs in 4/5Cb slices of mice. **d–g**, Trace records (**d**) and average values of AP threshold (**e**), RMP (**f**) and spike number (**g**) of PCs in 4/5Cb slices of mice. The brain slices were treated with THC (100 nM, 5 min) and ethanol (20 mM, 5 min), either alone or in combination. Values are represented as means ± s.e.m., *n* per group. Exact *P* values are shown. Statistical differences were determined by a one-way ANOVA followed by Tukey's post hoc multiple-comparison test.

increased after the AR test (Fig. 1e,f); however, of all the anterior cerebellar lobules, only lobules 4/5 (4/5Cb) showed a significant decrease in c-Fos expression in response to THC and ethanol combination, suggesting a critical role of 4/5Cb in the SETEM (Fig. 1e,f). We then examined whether ethanol promotes THC actions directly in 4/5Cb. THC (5 µg in 1 µl) was microinjected into 4/5Cb (intra-4/5Cb) through permanently implanted stainless steel guide cannulas 5 min before i.p. various doses of ethanol administration (Fig. 1g). This combination of THC and ethanol still significantly induced the SETEM in mice (Fig. 1h and Extended Data Fig. 2d,e).

To explore the functional role of 4/5Cb in motor coordination, we virally expressed a pharmacogenetic neural inhibitor hM4Di–mCitrine (AAV2/9–hSyn–hM4Di–mCitrine) or a control enhanced green fluorescent protein (EGFP) (AAV2/9–hSyn–EGFP) in the 4/5Cb of mice[30] (Fig. 1i). Histological analysis confirmed that hM4Di–mCitrine and EGFP were largely confined to the 4/5Cb (Fig. 1j). Chemogenetic inactivation of 4/5Cb neurons by clozapine *N*-oxide (CNO), an engineered ligand of hM4Di, indeed significantly reduced the 4/5Cb c-Fos expression level (Extended Data Fig. 2f) and motor coordination in mice transfected with hM4Di but not in those transfected with the control EGFP (Fig. 1k). Furthermore, chemogenetic activation of 4/5Cb neurons using AAV2/9–hSyn–hM3Dq–mCitrine restored c-Fos expression in the 4/5Cb (Fig. 1l and Extended Data Fig. 2g) and evidently inhibited the SETEM in mice carrying hM3Dq–mCitrine (Fig. 1m and Extended Data Fig. 3a,b), but it did not affect their basic motor skills (Extended Data Fig. 3c–e). Taken together, all these results suggest that 4/5Cb is a pivotal brain region for motor coordination and the SETEM.

THC and ethanol synergistically reduce PC excitability. PCs constitute the sole output of the cerebellar cortex and their dysfunction is a hallmark of motor incoordination[31]. We therefore examined whether THC and ethanol alter the electrophysiological properties of 4/5Cb PCs. To achieve this, we conducted whole-cell patch-clamp recordings of miniature excitatory postsynaptic currents (mEPSCs) of the PCs in the 4/5Cb. Combined incubation of low-dose THC (100 nM) and ethanol (20 mM) significantly reduced the frequency, but not amplitude, of the mEPSCs of PCs (Fig. 2a–c), indicating a presynaptic change. It is worth noting that, at such low doses, either THC or ethanol alone did not affect the mEPSCs (Fig. 2a–c). We also investigated the overall incoming inhibitory events in 4/5Cb PCs by measuring miniature inhibitory synaptic currents (mIPSCs). The results showed that neither the frequency nor the amplitude of mIPSCs was affected by THC and ethanol, either alone or in combination (Extended Data Fig. 4).

Next, we conducted whole-cell patch-clamp recordings of electrically evoked action potential (AP) in 4/5Cb PCs. The combination of low-concentration THC and ethanol incubation caused a significant increase in AP threshold and rest membrane potential (RMP) and a notable decrease in the number of AP spikes (Fig. 2d–g). These parameters were not affected by either THC or ethanol alone. All these results demonstrate that THC and ethanol synergistically decrease PC excitability.

CB_1R and GlyR in the 4/5Cb contribute to the SETEM. THC interacts with multiple CNS targets, mostly membrane receptors such as $CB_{1/2}R$, GlyR and transient receptor potential vanilloid 2 (TRPV2)[11,12], which are widely distributed in the cerebellum[32–34]. We next performed pharmacological tests to identify the specific targets involved in the SETEM (Fig. 3a). Systemic administration of either the CB_1R antagonist AM251 (Fig. 3b and Extended Data Fig. 5a,b) or GlyR antagonist strychnine (Fig. 3c and Extended Data Fig. 5c) significantly diminished the SETEM in a dose-dependent manner, whereas the CB_2R antagonist AM630 (Fig. 3d and Extended Data Fig. 5d) and TRPV2 antagonist tranilast (Fig. 3e and Extended Data Fig. 5e) did not affect the various doses of ethanol-associated SETEM (Extended Data Fig. 5f–i), suggesting specific involvement of CB_1R and GlyR, but not CB_2R or TRPV2, in the SETEM.

We next performed local microinjection to examine the role of CB_1R in the 4/5Cb in the SETEM (Fig. 3f). Intra-4/5Cb injection of AM251 significantly inhibited the SETEM (Fig. 3g and Extended Data Fig. 5j). Previous studies indicated that Serine 296 of GlyRα1 is a critical site for cannabinoid–GlyR interaction[20,35–39]. We therefore verified the role of 4/5Cb GlyRα1 in the SETEM using GlyRα1 S296A knock-in ($GlyR\alpha1^{S296A}$) mice (Fig. 3h). The synergistic effect of THC and ethanol was significantly inhibited in mice carrying the

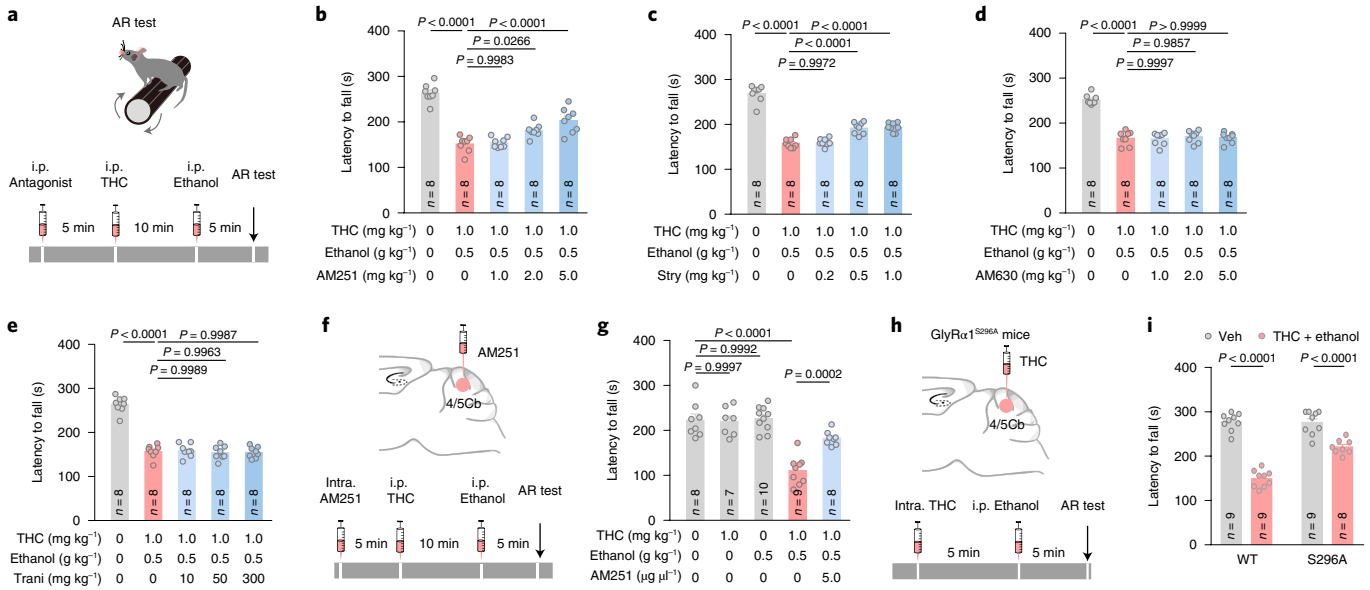

Fig. 3 | Pharmacological identification of drug targets in the 4/5Cb that are involved in the SETEM. a, Schematic showing the timeline of systemic drug administration and AR procedure. **b**–**e**, Effects of AM251 (i.p. 1.0, 2.0 and 5.0 mg kg^{-1}) (**b**), strychnine (i.p. 0.2, 0.5 and 1.0 mg kg^{-1}) (**c**), AM630 (i.p. 1.0, 2.0 and 5.0 mg kg^{-1}) (**d**) and tranilast (i.p. 10, 50 and 300 mg kg^{-1}) (**e**) on the SETEM caused by THC (i.p. 1.0 mg kg^{-1}) and ethanol (i.p. 0.5 g kg^{-1}) combination in mice. Stry, strychnine; Trani, tranilast. **f**, Schematic showing the timeline of intra-4/5Cb AM251 and systemic THC and ethanol administration and AR procedure. **g**, Effects of AM251 (intra-4/5Cb., 5 μg μl^{-1}) on the SETEM caused by THC (i.p. 1.0 mg kg^{-1}) and ethanol (i.p. 0.5 g kg^{-1}) combination in mice. **h**, Schematic showing the timeline of intra-4/5Cb THC and i.p. ethanol administration and AR procedure in GlyRα1^{S296A} transgenic mice. **i**, The SETEM caused by THC (intra-THC, 5 μg μl^{-1}) and ethanol (i.p. 0.5 g kg^{-1}) combination in GlyRα1^{WT} and GlyRα1^{S296A} mice. Values are represented as mean ± s.e.m., *n* per group. Exact *P* values are shown. Statistical differences were determined by a one-way ANOVA followed by Tukey's post hoc multiple-comparison test (**b**–**e**,**g**) or a two-way ANOVA followed by followed by Tukey's post hoc multiple-comparison test (**i**).

GlyRα1^{S296A} mutation (Fig. 3i and Extended Data Fig. 5k–m). Taken together, these results indicate that CB_1R and GlyR in the 4/5Cb may act as the primary targets of THC and ethanol to produce the SETEM.

4/5Cb CB_1R mediates the inactivation of PCs through a presynaptic mechanism. Next, we examined whether blocking CB_1R in the 4/5Cb can affect the synergistic effect of THC and ethanol on PC excitability. The THC and ethanol combination significantly increased the AP threshold and RMP and decreased the AP spike number, suggesting inactivation of PC neuronal function. Such effect of THC and ethanol was significantly inhibited by pre-incubation of AM251, as reflected by the significantly reduced AP threshold and RMP and increased number of AP spikes (Fig. 4a–d).

PCs have been reported to receive the majority of excitatory inputs from parallel fibers of granule cells in the cerebellar granule layer and climbing fibers of neurons in the inferior olive[40]. We next recorded the mEPSCs of 4/5Cb PCs. As demonstrated above, combined use of THC and ethanol significantly reduced the mEPSC frequency, but not amplitude (Fig. 4e–g), suggesting a presynaptic impairment of glutamate release. This reduction in mEPSC frequency was largely restored by AM251 (Fig. 4e–g). Thus, these results suggest a role of CB_1R in mediating the presynaptic inhibition of excitatory transmission caused by THC plus ethanol, which possibly leads to the inactivation of PCs and the subsequent SETEM.

4/5Cb GlyR mediates the inactivation of PC through an extrasynaptic mechanism. The GlyR, an important target of cannabinoids[16,17], has been reported to be distributed widely in the cerebellum[34]. We next used GlyRα1^{S296A} mutant mice to block the interaction between THC and GlyR[41,42]. Treatment with THC and ethanol at low concentrations significantly increased the AP threshold and RMP and decreased the number of AP spikes in PCs of GlyRα1^{WT} mice (Fig. 5a–d). These effects were significantly diminished in the GlyRα1^{S296A} mice, suggesting that specific blockade of the cannabinoid–GlyR interaction could restore the activity of PCs suppressed by the combined use of THC and ethanol (Fig. 5a–d).

The distribution of GlyR in 4/5Cb PCs was then determined by patch-clamp slice recording. Puffing glycine induced obvious strychnine-sensitive currents (I_{Gly}) in all (45 of 45) measured PCs in the cerebellar slice, suggesting that all PCs express GlyR (Fig. 5e). Glycinergic spontaneous inhibitory postsynaptic currents (sIPSCs) were detected in fewer than 3% of all measured PCs (1 of 45), indicating that GlyR is not usually located in the postsynaptic site of 4/5Cb PCs (Fig. 5f). Meanwhile, puffing strychnine induced small but obvious tonic currents (I_{tonic}), which are generally mediated by extrasynaptic ion channels, in about 97% (44 of 45) of PCs, suggesting that most GlyRs on PCs are extrasynaptic (Fig. 5g).

We next examined whether the extrasynaptic GlyRs (esGlyRs) are synergistically regulated by THC and ethanol. Although pre-incubation with either THC or ethanol alone at low concentrations failed to affect I_{tonic}, their combination caused significant potentiation of the I_{tonic} in the 4/5Cb PCs (Fig. 5h). This potentiation was considerably blocked by the S296A mutation of GlyRα1 in transgenic mice (Fig. 5i). Taken together, these results demonstrate that the function of esGlyR is synergistically boosted by THC plus ethanol, very likely leading to the inactivation of 4/5Cb PCs that results in the SETEM.

Ethanol elevates the THC level in the cell membrane. Cannabinoids are characterized by high lipophilicity and are primarily distributed in the cell membrane[43,44]. A question that has so far remained unsolved is how ethanol enhances THC actions at the cellular level. We therefore directly conjugated the THC compound with cyanine 7 (Cy7), a

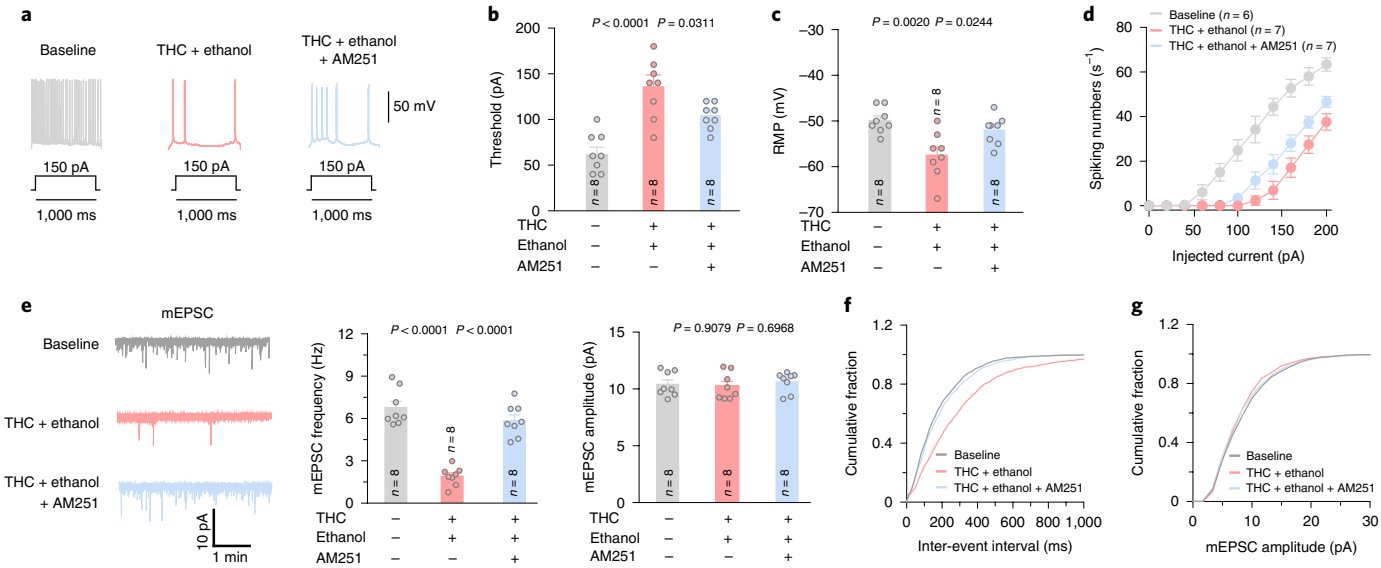

Fig. 4 | Effects of a CB_1R antagonist on the changes in PC neuronal excitability and mEPSCs caused by THC and ethanol combination. a–d, Trace records (**a**) and average values of AP threshold (**b**), RMP (**c**) and spike numbers (**d**) of PCs in 4/5Cb of mice. The slices were treated with THC (100 nM, 5 min) and ethanol (20 mM, 5 min) in combination, with or without AM251 (10 μM, 5 min). **e**, Trace records, average frequency and amplitude of mEPSCs of PCs in 4/5Cb slices of mice. The slices were treated with THC (100 nM, 5 min) and ethanol (20 mM, 5 min) in combination, with or without AM251 (10 μM, 5 min). **f**,**g**, Cumulative probability plot for the inter-event interval (**f**) and the amplitudes (**g**) for mEPSCs of PCs in 4/5Cb slices of mice. Values are represented as means ± s.e.m., *n* per group. Exact *P* values are shown. Statistical differences were determined by a one-way ANOVA followed by Tukey's post hoc multiple-comparison test.

classic near-infrared fluorophore, to visualize and quantify the THC in HEK293 cells and the neuroblastoma cell line Neuro 2A (N2A) using flow cytometry (Fig. 6a). THC–Cy7 still induced a remarkable decrease in intracellular cAMP concentration in HEK293 cells expressing CB_1R and a significant potentiation of puffed glycine-triggered currents (I_{Gly}) in HEK293 cells expressing GlyRα1, suggesting that the Cy7-conjugation does not affect the pharmacological properties of THC (Fig. 6b,c). HEK293 and N2A cells were incubated with THC–Cy7 for 1 h and then analyzed by standard flow cytometry (SFC) (Fig. 6d and Extended Data Fig. 6a–h). The median fluorescence intensity of HEK293 cells or N2A cells incubated with THC–Cy7 was significantly larger than that of cells incubated with Cy7 only (Fig. 6e–h and Extended Data Fig. 6i–l). More notably, ethanol treatments indeed induced a considerable increase in THC–Cy7 levels in HEK293 and N2A cells (Fig. 6e–h).

We further examined the cellular level of THC using high-performance liquid chromatography mass spectrometry (HPLC–MS) (Fig. 6i). HEK293 and N2A cells were incubated with various doses of THC to construct a calibration curve for method validation (Extended Data Fig. 6m,n). Three major fragments of THC at m/z = 179, 191 and 245 were identified in the incubation buffer (Extended Data Fig. 6o,p). The THC contents in the HEK293 and N2A cells were then obtained by subtracting the amount of THC in the supernatant. The results showed that ethanol remarkably increased the level of THC in the whole-cell lysate, as reflected by a significantly reduced THC concentration in the incubation buffer (Fig. 6j–m).

We then analyzed the membrane-anchored THC–Cy7 in HEK293 and N2A cells using imaging flow cytometry (IFC)[45]. Based on IFC, the focused HEK293 or N2A cells were selected using gradient root mean square (RMS) (Extended Data Fig. 7a,b) and then gated to single cells based on area versus aspect ratio (Extended Data Fig. 7c,d). These single-focused cells were then used for membrane fluorescence analysis. Ethanol co-incubation significantly enhanced the membrane fluorescence intensity of THC–Cy7 in HEK293 and N2A cells (Fig.6n–s and Extended Data Fig. 7e–j), indicating that ethanol promotes membrane accumulation of THC.

Ethanol boosts THC levels in the brain. To examine the effect of ethanol on THC distribution in the brain, we conducted live animal imaging, which has been regarded as an efficient tool for real-time visualization of drug distribution in live animals (Fig. 7a). Following i.p. injection, the fluorescence of THC–Cy7 was observed in the brain and other organs (Extended Data Fig. 8a). Various doses of ethanol treatments accelerated the accumulation of THC in the brain and caused significant increases in the intensity of THC during the 120 min after the THC–Cy7 injection (Fig. 7b,c and Extended Data Fig. 8b–e), suggesting that ethanol promotes the ability of THC crossing the blood–brain barrier (BBB).

We then performed additional in vitro and in vivo experiments to evaluate the effect of low-dose ethanol on BBB permeability using a FITC-dextran trans-epithelial permeability assay[46]. We first constructed the in vitro BBB model using bEnd.3 endothelial cells (Extended Data Fig. 8f), which have been evidenced to be a convenient and useful model for evaluating BBB function[47–49]. The results showed that the low-dose ethanol (20 mM, 5 min) significantly increased the permeability of FITC-dextran (1.0 mg kg^{-1}, 1 h) crossing the layer of endothelial cells, reflected by the increased FITC intensity in the lower chamber of the Transwell (Extended Data Fig. 8g). To evaluate the in vivo effect of low-dose ethanol on BBB, FITC-dextran (i.p. 50 mg kg^{-1}) was injected into C57BL/6J mice. After circulating for 1 h, the mice were injected with saline or ethanol (i.p. 0.5 g kg^{-1}) and then were killed 5 min after ethanol administration. The immunofluorescence staining and brain homogenization results showed that the low-dose ethanol significantly increased the FITC intensity in the various brain regions, especially in the cerebellum (Extended Data Fig. 8h,i). Taken together, these results provided evidence that low-dose ethanol in a short period of time indeed increases the BBB permeability, which likely leads to the elevated brain level of THC.

Next, we performed HPLC–MS to measure the concentration of THC in the blood and brain tissue after i.p. THC injection (Fig. 7d). Various doses of standard THC were used to construct a calibration curve for method validation (Extended Data Fig. 8j). Three major

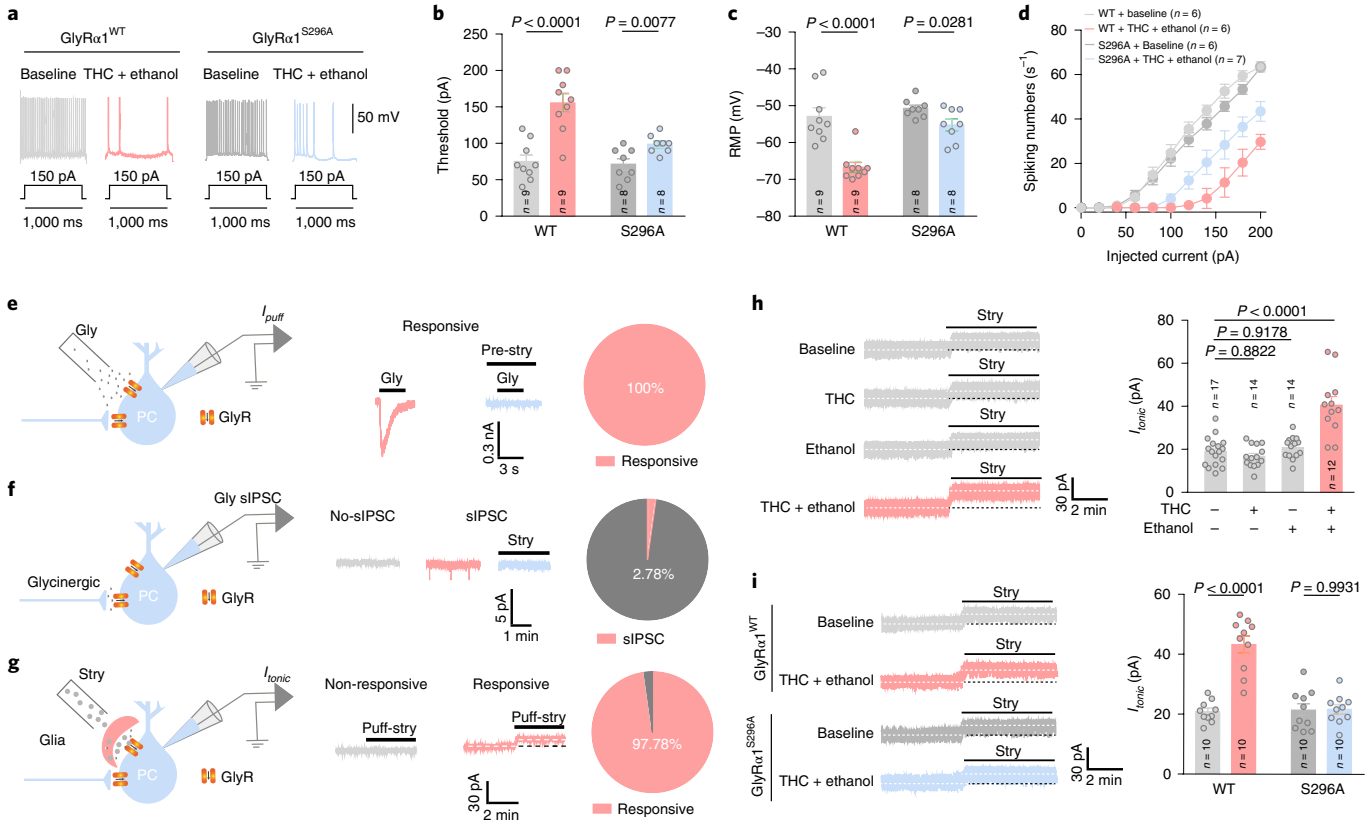

Fig. 5 | Effects of THC and ethanol combination on the function of esGlyR. a–d, Trace records (**a**) and average values of AP threshold (**b**), RMP (**c**) and spike number (**d**) of PCs in 4/5Cb slices of GlyRα1^{WT} and GlyRα1^{S296A} mice. The brain slices were treated with THC (100 nM, 5 min) and ethanol (20 mM, 5 min) in combination. **e**, Schematic showing electrophysiological recording of I_{Gly} in 4/5Cb slices of mice (left). Representative trace currents of I_{Gly} in responsive (red) or non-responsive neurons (gray) (middle). Pie graphs showing ratios of responsive (red) and non-responsive neurons (gray) (right). **f**, Schematic showing electrophysiological recording of glycinergic sIPSCs in 4/5Cb slices of mice (left). Representative trace currents of glycinergic sIPSCs in responsive (red) or non-responsive neurons (gray) (middle). Pie graphs showing ratios of responsive (red) and non-responsive neurons (gray) (right). **g**, Schematic showing electrophysiological recording of I_{tonic} in 4/5Cb slices of mice (left). Representative trace currents of I_{tonic} in responsive (red) or non-responsive neurons (gray) (middle). Pie graphs showing ratios of responsive (red) and non-responsive neurons (gray) (right). **h**, Trace records and average values of I_{tonic} of PCs in 4/5Cb slices of mice. **i**, Trace records and average values of I_{tonic} of PCs in 4/5Cb slices of GlyRα1^{WT} and GlyRα1^{S296A} mice. Values are represented as mean ± s.e.m., *n* per group. Exact *P* values are shown. Statistical differences were determined by a one-way ANOVA followed by Tukey's post hoc multiple-comparison test (**h**) or a two-way ANOVA followed by Tukey's post hoc multiple-comparison test (**b**,**c**,**i**).

characteristic peaks of THC at m/z = 179, 191 and 245 were detected in the brain tissue and plasma (Fig. 7e and Extended Data Fig. 8k). Ethanol significantly increased the intensity of plasma THC over the 45 min, especially during the first 15 min, after THC injection (Extended Data Fig. 8l). Furthermore, the THC intensity in the cerebellum of mice co-treated with THC and ethanol was considerably higher than that in mice treated with THC alone (Fig. 7f,g and Extended Data Fig. 8m). Together, these results demonstrate that ethanol can facilitate THC accumulation in the brain, possibly by boosting the BBB permeability of THC.

A synthetic cannabinoid specifically disrupting THC–GlyR interaction inhibits the SETEM. The above results indicate that antagonists against CB_1R or GlyR can efficiently inhibit the SETEM, making them potential therapeutic treatments for the psychiatric toxicity caused by THC and alcohol combination; however, antagonism of CB_1R or GlyR can inevitably induce a series of psychiatric side effects such as anxiety, depression and seizure[20,50,51]. Di-desoxy-THC (DDT), a chemically modified THC with both hydroxyl and oxygen groups removed (Fig. 8a and Extended Data Fig. 9a), has been shown to selectively disrupt the cannabinoid–GlyR interaction without affecting the basic functions of CB_1R and GlyR[35–37]. We therefore examined the therapeutic effects of DDT on the SETEM and whether DDT causes any side effects related to CB_1R and GlyR. Electrophysiological slice recording showed that DDT significantly suppressed the THC and ethanol combination-induced potentiation of 4/5Cb PC esGlyR-mediated I_{tonic} (Fig. 8b). DDT also considerably inhibited the hyperexcitability of PCs caused by THC and ethanol combination, as reflected by the restored AP threshold, RMP and number of AP spikes (Fig. 8c–f). Furthermore, DDT significantly diminished the various doses of ethanol-associated SETEM in a dose-dependent manner (Fig. 8g,h and Extended Data Fig. 9b) without affecting ethanol alone induced motor incoordination (Extended Data Fig. 9c) and basic motor coordination of mice (Fig. 8i).

Chronic ethanol exposure (CEE) is a common clinical alcohol abuse condition and cannabis is always co-used in chronic alcohol users[52,53]. We thus constructed the CEE model and examined the effect of CEE on SETEM (Extended Data Fig. 9d). Acute i.p. administration of THC also caused SETEM in CEE mice (Extended Data Fig. 9d–f). Such CEE-associated SETEM could be significantly inhibited by DDT (Extended Data Fig. 9e) and AM251 (Extended Data Fig. 9f), suggesting a similar involvement of GlyR and CB_1R in the SETEM associated with CEE and a potential therapeutic role of DDT in clinical situation of long-term alcohol abuse with cannabinoid use.

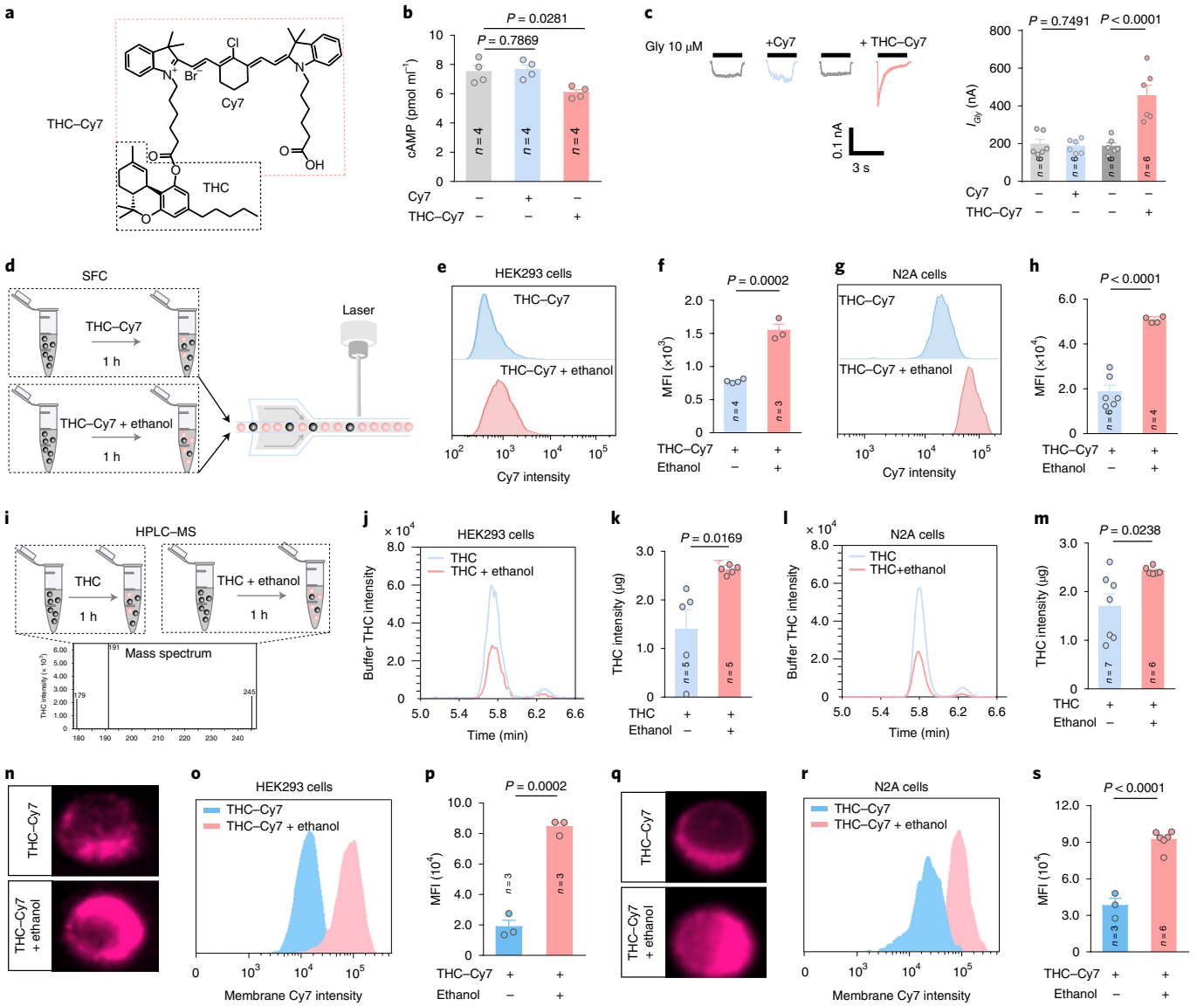

Fig. 6 | Effects of ethanol on THC distribution in HEK293 and N2A cells. a, The chemical structure THC-Cy7. **b**, The concentration of cAMP in HEK293 cell lysate pre-incubated with Cy7 (10 μM, 15 min) or THC-Cy7 (10 μM, 15 min). **c**, Representative trace records and average values of I_{Gly} activated by 10 μM glycine in HEK-293 cells expressing the GlyRα1 subunit with or without Cy7 (10 μM) or THC-Cy7 (10 μM) pre-incubation. **d**, Schematic showing the process for THC-Cy7 treatment and the subsequent SFC experiment. The cells were treated with THC-Cy7 (10 μM, 1h) or THC-Cy7 (10 μM, 1h) and ethanol (20 mM, 1h) in combination. **e**–**h**, Histograms and quantitative analysis of MFI obtained from SFC analysis of HEK293 cells (**e**,**f**) or N2A (**g**,**h**) cells. MFI, mean fluorescence intensity. **i**, Schematic showing the process for THC treatment and the subsequent HPLC-MS experiment. **j**, Mass spectra of THC obtained from HPLC-MS analysis of HEK293 cell buffer. **k**, Quantification of intensities of THC obtained from HPLC-MS analysis of HEK293 cells. THC content in the HEK293 cells was obtained by subtracting the amount of THC in the buffer. **l**, Mass spectra of THC obtained from HPLC-MS analysis of N2A cell buffer. **m**, Quantification of the intensities of THC obtained from HPLC-MS analysis of N2A cells. **n**–**s**, Representative cell images, histograms and quantitative analysis of MFI obtained from IFC of HEK293 cells (**n**–**p**) or N2A cells (**q**–**s**) treated with THC-Cy7 (10 μM, 1h) alone or THC-Cy7 (10 μM, 1h) with ethanol (20 mM, 1h) in combination. Values are represented as mean ± s.e.m., *n* per group. Exact *P* values are shown. Statistical differences were determined by a one-way ANOVA followed by Tukey's post hoc multiple-comparison test (**b**,**c**) or a two-sided unpaired *t*-test (**f**–**s**).

We next evaluated the possible effects of DDT on a series of behaviors including the startle reflex, righting reflex, locomotor activity and emotion, which have been reported to be influenced by antagonism of GlyR or CB_1R[50,54]. DDT from low to high doses had no effects on the acoustic startle response (Fig. 8j), the righting reflex time (Fig. 8k), the percentage of open arm entries and time in elevated plus maze tests (Fig. 8l–n) and the percentage of center zone entries, time and traveling distance in open field tests (Fig. 8o–s). Furthermore, the DDT did not affect many other behavioral manifestations of mice such as gait, grip strength, body temperature and food intake, suggesting the nontoxicity of DDT (Extended Data Fig. 9g–m). Taken together, these results suggest that DDT can be regarded as an effective candidate medication for preventing and treating the SETEM without inducing any CB_1R/GlyR-related side effects.

Discussion

THC and alcohol, the two most commonly used psychoactive drugs, have been reported to be frequently used in combination and to cause synergistic psychoactive effects[3]. In the present study, we provided several lines of evidence regarding the mechanism by

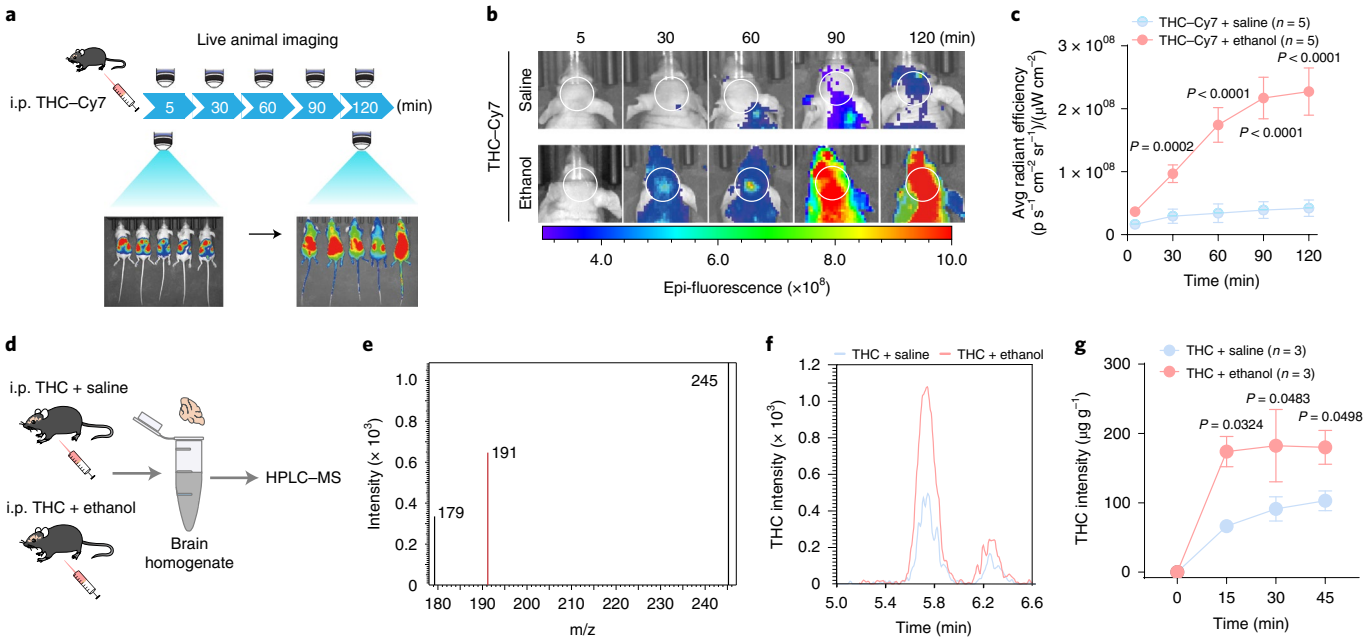

Fig. 7 | Effects of ethanol on THC distribution in the brain. a, Schematic of live animal imaging of THC-Cy7. The mice were treated with THC-Cy7 (10 mg kg^{-1}) or THC-Cy7 (10 mg kg^{-1}) with ethanol (0.5 g kg^{-1}) in combination. **b**, Representative fluorescence images of mice. Five time points, namely 5 min, 30 min, 60 min, 90 min and 120 min after ethanol injection, were selected for imaging. The brain area in the white circle was designated as the region of interest. **c**, Brain fluorescence intensity of THC-Cy7 measured at 5 min, 30 min, 60 min, 90 min and 120 min after ethanol injection. **d**, Schematic diagram showing the process of THC administration and HPLC–MS measurement. Mice were treated with THC (10 mg kg^{-1}) or THC (10 mg kg^{-1}) and ethanol (0.5 g kg^{-1}) in combination. **e**, Representative mass spectra of THC obtained from cerebellum tissue lysis. **f**, Mass spectra of THC obtained from HPLC–MS analysis of cerebellum tissue lysates of mice. **g**, Quantitative analysis of mouse cerebellar THC intensity. Four time points after drug administration were selected for HPLC–MS: 0 min, 15 min, 30 min and 45 min. Values are represented as mean ± s.e.m., *n* per group. Exact *P* values are shown. Statistical differences were determined by a two-way ANOVA followed by Tukey's post hoc multiple-comparison test.

which THC and alcohol synergistically cause severe motor incoordination. For instance, ethanol enhances the ability of THC to cross the BBB, leading to elevated brain THC levels. Furthermore, ethanol increases the cellular membrane level of THC, which in turn potentiates function of synaptic receptors including presynaptic CB_1R and esGlyR in the cerebellum and therefore synergistically inactivates the cerebellar PCs, finally leading to motor incoordination. In short, the SETEM seems to be a comprehensive result of the ethanol–THC interaction at multiple levels, from the molecular level to the cellular level and to the brain circuit level.

Presynaptic CB_1Rs and postsynaptic esGlyRs are identified as two critical targets of THC and ethanol in SETEM in the present study. Blocking either one of the two targets partially reverses the neuronal excitability caused by THC and ethanol combination and suppresses the SETEM. Nevertheless, some other targets such as cerebellar adenosinergic A1 receptor and nicotinic-cholinergic receptors have also been reported to be involved in cannabinoid-induced motor incoordination[7,55,56]; however, whether these targets also contribute to SETEM is still unknown and remains to be further investigated.

Consistent with our findings, emerging evidence also shows that both acute and chronic ethanol usage can increase the permeability of the BBB[57–60]. For example, acute ethanol administration enhances the BBB permeability of catecholamines[57]. Ethanol leads to dysfunction of tight junctions and the BBB via activation of myosin light chain kinase[59]. Alcohol abuse-induced oxidative stress in brain microvascular endothelial cells can lead to BBB breakdown[60]. Furthermore, as reported by previous clinical studies[61], the present study also finds that ethanol significantly increases the circulatory THC level. Considering our finding that ethanol can enhance the BBB permeability of THC, higher levels of ethanol in the blood may be the basis for more THC entering the brain. Thus, in the presence of ethanol, a large amount of THC may cross the BBB and act in regions of the brain including the cerebellum, therefore leading to more severe psychoactive effects.

In addition to acting on the cerebellum, THC has also been reported to cause motor incoordination via disrupting autophagy in striatum[62]. It is likely that such effect in striatum may also contribute to the SETEM, as ethanol seems to increase the THC level in the whole brain. Although the present study finds that ethanol and THC combination did not affect the c-Fos expression of striatum, such combination may synergistically affect autophagy in the striatum and thereby lead to the SETEM; however, whether autophagy in the striatum is involved in the SETEM still needs further research.

Cannabinoids, as lipophilic molecules, can remain in or diffuse across the cell membrane[43,44]. Our results have shown that ethanol can increase membrane THC levels. Consistent with this finding, there is a large amount of evidence that ethanol can influence the physical structure of the cell membrane, causing the phospholipid bilayers to be more fluid and permeable[63–65]. For instance, acute ethanol exposure changes the lipid bilayer free volume and disrupts the phospholipid acyl chain packing of the erythrocyte, mitochondrial and synaptosomal membranes, causing the membrane to be looser[65]. Thus, it is likely that the ethanol-induced membrane structural change is one primary cause of the increased THC concentration in the cell membrane.

Our results show that ethanol significantly increases the brain THC level, resulting in severe motor incoordination. In addition, accumulation of THC in the brain can cause many other adverse psychoactive effects, including anxiety, addiction, illusion and hypothermia[11,12,66]. Thus, the harmful effects of the combined use of ethanol and cannabis can be manifold. Based on our findings, several emergency strategies may be effective for clinically treating

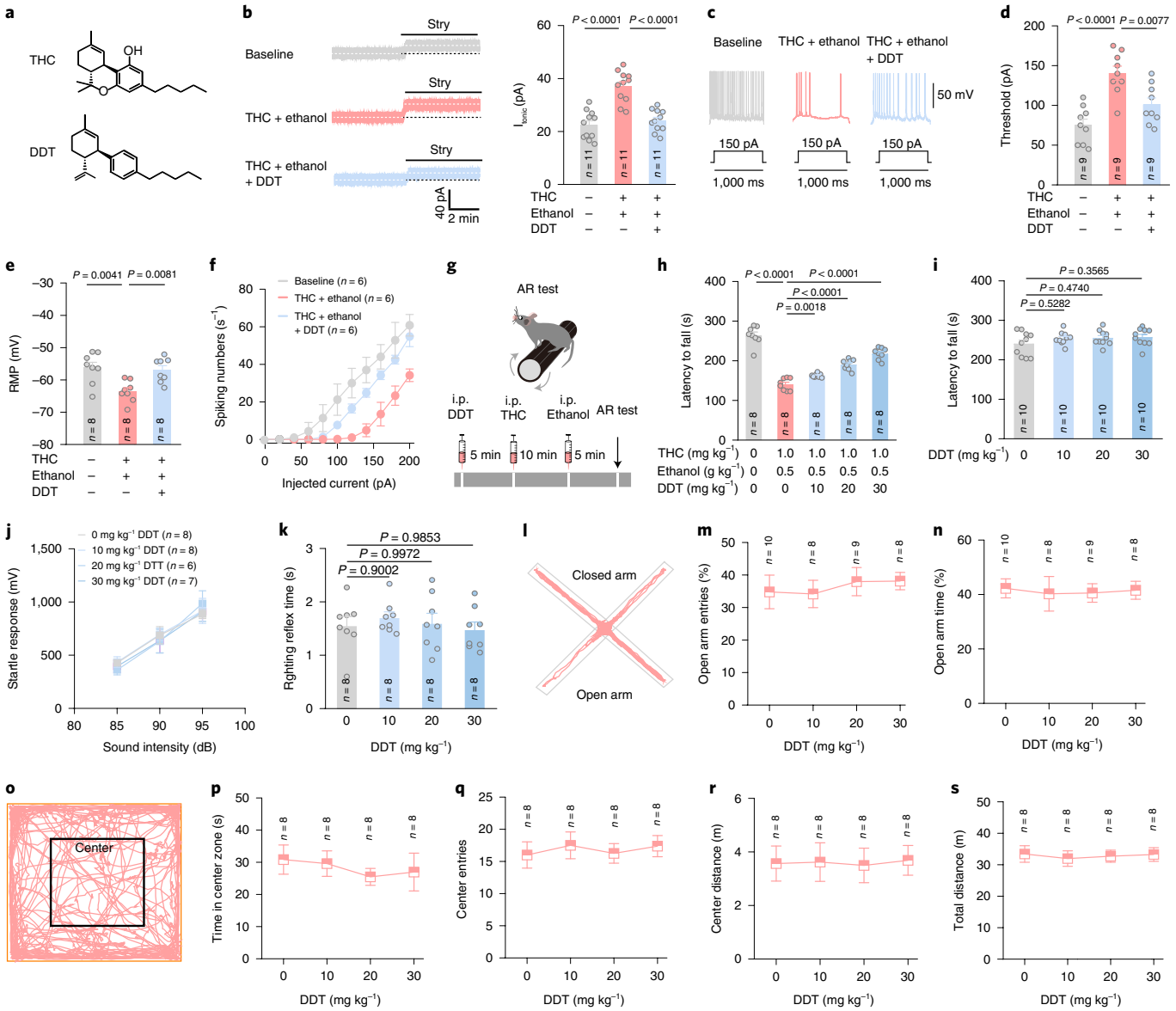

Fig. 8 | Effects of DDT on PC activity, the SETEM and other behaviors. a, Chemical structures of THC and DDT. **b**, Trace records and average values of I_{tonic} of PCs in 4/5Cb slices of mice. The slices were treated with THC (100 nM, 5 min) and ethanol (20 mM, 5 min) in combination, with or without DDT (10 μM, 5 min). **c**–**f**, Trace records (**c**) and average values of AP threshold (**d**), RMP (**e**) and spike number (**f**) of PCs in 4/5Cb slices of mice. **g**, Schematic showing the timeline of systemic drug administration and AR procedure. **h**, Effects of DDT (i.p. 10, 20 and 30 mg kg^{-1}) on the SETEM caused by THC (i.p. 1.0 mg kg^{-1}) and ethanol (i.p. 0.5 g kg^{-1}) combination. **i**, Effects of DDT on AR latency. **j**, Average values of startle responses induced by white noise at 85, 90 and 95 dB in mice injected with DDT. **k**, Average values of righting reflex time of mice injected with DDT. **l**, Representative trajectories of mice injected with DDT in the elevated plus maze test. **m**,**n**, The percentage of open arm entries (**m**) and open arm time (**n**) of mice injected with DDT in the elevated plus maze test. **o**, Representative trajectories of mice injected with DDT in the open field test. **p**,**q**, Average values of center zone time (**p**) and entries (**q**) of mice injected with DDT in the open field test. **r**,**s**, The center zone distance (**r**) and total distance (**s**) of mice injected with DDT in the open field test. Different cohorts of mice were used for each behavioral test. Values are represented as mean ± s.e.m., *n* per group. Exact *P* values are shown. Statistical differences were determined by one-way ANOVA followed by Tukey's post hoc multiple-comparison test.

the acute intoxication caused by THC and ethanol combination, such as intravenous injections to dilute blood ethanol, medications that can accelerate ethanol metabolism and drugs targeting CB_1R or GlyR; however, GlyR antagonists are generally neurotoxic and can induce neuronal hyperexcitability and seizure[20,51,67]. CB_1R antagonists also cause a series of psychiatric side effects such as anxiety, depression and suicidal ideation[50,68]. Thus, DDT, a compound specifically disrupting THC–GlyR interaction without affecting basic CB_1R and GlyR functions, as revealed by this study and our previous studies[35–37], may be a potential therapeutic strategy for blocking the neural toxicity caused by THC and ethanol combination, with minimal side effects.

Methods

Animals. All animal procedures were approved by and performed in accordance with the guidelines of the Institutional Animal Care and Use Committee of University of Science & Technology of China (permit USTCACUC1901009). Male (unless otherwise indicated) C57BL/6J (8 weeks old) (cat. no. 219) obtained from Vital River Laboratory Animal Technology Co. were used for various behavioral tests, immunohistochemistry, electrophysiological recording and HPLC–MS. BALB/c Nude mice (cat. no. 401) of the same age and source with C57BL/6J

mice were used for live animal imaging. Male GlyRα1^{S296A} mice (8 weeks old) and their wild-type littermates were also used for electrophysiological recording and behavioral tests. Genotyping of the GlyRα1^{S296A} mice was performed using the following primers: forward: 5′-GAATCTTCCAGGCAACATTTCAG-3′; reverse: 5′-AGTATCCCACCAAGCC AGTCTTT-3′. All mice were bred and housed under a specific-pathogen-free conditions with 12-h dark–light cycle at 21 ± 1 °C and 55–60% humidity and provided with ad libitum access to water and food (Jiangsu Xietong Pharmaceutical Bio-engineering Co., cat. no. 1010088).

Cell cultures. HEK293 cell line (American Type Culture Collection, ATCC) was a gift from T. Xue (University of Science & Technology of China) and accompanied by authentication documents verifying the identity according to their short tandem repeat profiles. HEK293 cells and N2A neuronal cells were cultured in Dulbecco's modified Eagle's medium (HyClone). bEnd.3 cells (ATCC) were cultured in Opti-MEM medium. All cell lines were routinely split with fresh medium every 3–5 d, when ~80 % confluency was reached. All the media were supplemented with 10 % fetal bovine serum (FBS; Gibco), penicillin (100 U ml^{-1}) and streptomycin (100 μg ml^{-1}). All cell lines were incubated in a humidified atmosphere consisting of 95% air and 5% CO_2 at 37 °C.

Blood ethanol concentration. Male C57BL/6J mice (8 weeks old) (cat. no. 219) were i.p. injected with various doses (0.5, 1.0 and 2.0 g kg^{-1}) of ethanol either alone or in combination with THC (1.0 mg kg^{-1}). THC was i.p. injected 10 min before ethanol administration. The mice were killed and the blood was collected at the time points of 0 min, 5 min, 15 min and 45 min after ethanol administration. The blood was then centrifuged at 10,000*g* for 10 min at 4 °C and the plasma was collected. Plasma ethanol concentration was measured using an Ethanol Assay kit (ab65343, Abcam) according to the manufacturer's protocol and expressed as mg dl^{-1}.

Mice BBB permeability. FITC-dextran BBB permeability assay was performed as previously described[69]. To assess BBB permeability, male C57BL/6J mice (8 weeks old) (cat. no. 219) were i.p. injected with 50 mg kg^{-1} FITC-dextran (MCE, 60842-46-8, 10 kDa). After circulating for 1 h, the mice were i.p. injected with saline or ethanol (0.5 g kg^{-1}) and the mice were killed by transcardial perfusion with 0.1 M PBS 5 min after ethanol administration. One hemisphere of the cerebellum was isolated, weighed and homogenized in 1% Triton X-100 in 0.1 M PBS. FITC-dextran fluorescence (excitation 490 nm and emission 520 nm) was then quantified using a fluorescence microplate reader (Synergy H1, BioTek). For the visualization of fluorescence penetration in the brain sections, the contralateral hemisphere was post-fixed in 4% PFA for 12 h and then sectioned to 40-μm sagittal slices and imaged with Tissue FACXS System with a ×20 objective (Tissue Gnostics).

FITC-dextran transendothelial permeability assay. The FITC-dextran transendothelial permeability assay was performed as previously described[46]. Briefly, bEnd.3 cells (ATCC) were seeded at a density of 2×10^4 cells per well on the upper chamber of collagen-coated Transwell in 12-well plates (Corning Transwell) and cultured with Opti-MEM medium with 10% FBS. The cell monolayer usually reaches confluency after 2 d. The integrity of the cell monolayer was evaluated by measuring the transendothelial electrical resistance (TEER) values using a Millicell-ERS voltohmmeter (Millipore). The cell monolayers with TEER values higher than 300 Ω cm^2 were used for the transmigration studies. Before 10 KD FITC-dextran (1.0 mg ml^{-1}) dissolved in phenol red-free Opti-MEM medium (Gibco, 11058021) was added in the upper chamber, culture medium in the lower chamber was replaced with phenol red-free Opti-MEM medium. FITC-dextran at 1.0 mg ml^{-1} was added to the upper chamber and then incubated for 1 h, followed by the incubation of ethanol at 20 mM for 5 min. Then 100 μl of serum-free medium were taken from the lower chamber and the fluorescence (excitation 490 nm and emission 520 nm) was then quantified using fluorescence microplate reader (Synergy H1, BioTek).

The synthesis of THC–Cy7. A solution of Cy7 (73.4 mg, 0.09 mmol), 4-dimethylaminopyridine (DMAP, 3.10 mg, 9.9 μmol) and 1-ethyl-3-(3-dimethyllaminopropyl) carbodiimide hydrochloride (EDC.HCl, 26.10 mg, 0.1125 mmol) in 3 ml freshly distilled DCM was purged with nitrogen under dark conditions. THC (27.9 mg, 0.09 mmol) was added and the mixture was stirred at room temperature overnight. The reaction was quenched with water and extracted with ethyl acetate. The organic phase was combined, dried over anhydrous magnesium sulfate and concentrated to a dark brown oil. The crude residue was purified by flash chromatography (20:1 ratio of DCM:methanol) to yield THC–Cy7 (33.10 mg, 35% yield, R_f 0.25 (10:1 ratio of DCM:methanol)) as a dark green viscous oil.

Standard flow cytometry. HEK293 and N2A cells were seeded at a density of 10^6 cells ml^{-1} in 35-mm dishes and allowed to grow to 70–80 % confluence. Both kinds of cells were washed with 1 ml ice-cooled 0.1 M PBS three times. Cells were then suspended with 1 ml ice-cooled 0.1 M PBS, collected in 1.5-ml tubes and centrifuged at 600*g* for 5 min. The supernatant was discarded and the pellet was re-suspended with 1 ml ice-cooled 0.1 M PBS. To accurately visualize the amounts of THC in the whole cell, THC–Cy7 at 10 μM was added in the suspended cells to incubate for 1 h at 37 °C, either alone or in combination with ethanol at 20 mM. As a control, Cy7 at 10 μM was also applied to incubate the cells in the same manner. After 1 h incubation, cells were immediately placed on ice and then centrifuged at 600*g* for 5 min at 4 °C. The layer of debris from the top of the tube was gently removed and cells were washed with 1 ml ice-cooled 0.1 M PBS three times. Cells were re-suspended with 1 ml ice-cooled 0.1 M PBS into clean tubes for flow cytometry. All tubes were placed on ice and vortexed for 5 s to completely dissociate the cells into a single-cell suspension. At least 5,000 events were recorded for each sample during flow cytometry analysis. Cells were gated based on FSC-A versus SSC-A parameters and these samples were chosen for fluorescence-activated cell sorting. The whole-cell fluorescence was measured and analyzed by a BD LSRFortessa X-20 cell analyzer equipped with 640 nm excitation laser with standard filter setup. Data were acquired using BD FACSDiva v.6 Software system (BD Biosciences) and then analyzed using FlowJo v.10 software.

Imaging flow cytometry. IFC was used to visualize THC–Cy7 or Cy7 intensity in the cell membrane. HEK293 and N2A cells were cultured and treated in the same way as for SFC. Bright-field channel was measured and at least 5,000 events of single cells were collected. All cell images were acquired in the INSOIRE software on the ImageStream Mark II Imaging Flow Cytometry (Amnis, Merck Millipore) at ×40 magnification with 640 nm lasers. Cell debris were gated out and the focused single cells were identified using the IDEAS v.6.2 software. Gradient RMS was first used to find the focused cells; gradient RMS is useful for the selection of focused images by measuring large changes of pixel values in the image and is computed using the average gradient of a pixel normalized for variations in intensity levels. Cells with a gradient RMS value between 40–100 were included for further analysis. The focused cells were then gated based on area (size of the focused cells) versus aspect ratio (minor axis divided by the major axis of the focused cells) to gate single cells. This population of single-focused cells was used for downstream membrane fluorescence intensity analysis. The membrane was defined by the Dilate module in the IDEAS v.6.2 software. The THC–Cy7 or Cy7 intensity in the membrane was analyzed in the IDEAS v.6.2 software. Raw data files of each processed sample were obtained using the IDEAS software platform.

Live animal imaging. Live animal imaging of male Balb/c nude mice (8 weeks old) (cat. no. 401) was conducted for in vivo imaging of THC–Cy7 and Cy7. Balb/c nude mice received i.p. injection of THC–Cy7 at 10 mg kg^{-1} or Cy7 at 10 mg kg^{-1}, either alone or in combination with ethanol at 0.5 g kg^{-1}, 1.0 g kg^{-1} and 2.0 g kg^{-1}. THC–Cy7 and Cy7 were i.p. injected 5 min after saline or ethanol i.p. administration. The mice were then anesthetized with isoflurane (RWD) and images were obtained in real-time at various time points after fluorescent reagent injection. Each mouse was imaged at 5 min, 30 min, 60 min, 90 min and 120 min after injection of ethanol administration. The dorsal side of each mouse was imaged. Live animal imaging was performed with a Xenogen IVIS Spectrum Imaging System (PerkinElmer). An ICG filter (excitation wavelength 745 nm and emission wavelength 820 nm) was used for acquiring Cy7 fluorescence imaging in vivo. Identical illumination settings, such as exposure time (auto), binning factor (8), f/stop (2) and fields of view (25 × 25 cm), were used for acquiring all images and fluorescence emission was normalized to photons per second per centimeter squared per steradian (p s^{-1} cm^{-2} sr^{-1}). The pseudocolor image represents the spatial distribution of photon counts within the animal. Regions of interest (ROIs) were manually defined. Background fluorescence was measured and subtracted by setting up a background measurement. Images were acquired and quantified using Living Image v2.5 software (PerkinElmer). The brain area was designated as the ROI and the ROI region was manually defined.

Drugs. Most chemicals, including glycine, ethanol, AM251, tranilast, strychnine and AM630 were achieved from Sigma-Aldrich. LC–MS-grade acetonitrile and methanol were purchased from Honeywell. All solutions were prepared the day before experiments with ultrapure water. In patch-clamp recordings, the agonists, modulators and antagonists were diluted before experiments with an external solution or artificial cerebrospinal fluid. THC and DDT were synthesized by USTC-Ruida Joint Laboratory according to the procedure described previously[35,70]. The chemical structure of THC was confirmed by means of electrospray ionization tandem mass spectrometry and 1H nuclear magnetic resonance analysis. THC and DDT was dissolved in ethanol before further dilution.

Statistical analysis. For behavioral tests, animals with different genotypes were picked randomly. For patch-clamp experiments, Purkinje neurons or transfected HEK293 cells were randomly picked for recordings. Data were statistically compared by one-way ANOVA, two-way ANOVA and unpaired Student's *t*-tests using GraphPad Prism v.8.0 (GraphPad Software), as indicated in figure legends. Average values are expressed as mean ± s.e.m.

Reporting summary. Further information on research design is available in the Nature Research Reporting Summary linked to this article.

Data availability

Source data are provided with this paper.

Received: 7 March 2022; Accepted: 3 August 2022;
Published online: 15 September 2022

References

1. Abrahao, K. P., Salinas, A. G. & Lovinger, D. M. Alcohol and the brain: neuronal molecular targets, synapses, and circuits. *Neuron* **96**, 1223–1238 (2017).
2. Hall, W. & Solowij, N. Adverse effects of cannabis. *Lancet* **352**, 1611–1616 (1998).
3. Yurasek, A. M., Aston, E. R. & Metrik, J. Co-use of alcohol and cannabis: a review. *Curr. Addict. Rep.* **4**, 184–193 (2017).
4. Ramaekers, J. G. Driving under the influence of cannabis: an increasing public health concern. *JAMA* **319**, 1433–1434 (2018).
5. Cole, T. B. & Saitz, R. Cannabis and impaired driving. *JAMA* **324**, 2163–2164 (2020).
6. Dubois, S., Mullen, N., Weaver, B. & Bedard, M. The combined effects of alcohol and cannabis on driving: Impact on crash risk. *Forensic Sci. Int.* **248**, 94–100 (2015).
7. Dar, M. S. Cerebellar CB(1) receptor mediation of Delta(9)-THC-induced motor incoordination and its potentiation by ethanol and modulation by the cerebellar adenosinergic A(1) receptor in the mouse. *Brain Res.* **864**, 186–194 (2000).
8. Funada, M., Takebayashi-Ohsawa, M. & Tomiyama, K. I. Synthetic cannabinoids enhanced ethanol-induced motor impairments through reduction of central glutamate neurotransmission. *Toxicol. Appl. Pharmacol.* **408**, 115283 (2020).
9. Singh, A., Stredny, C. M. & Loddenkemper, T. Pharmacotherapy for pediatric convulsive status epilepticus. *CNS Drugs* **34**, 47–63 (2020).
10. Hirvonen, J. et al. Reduced cannabinoid CB1 receptor binding in alcohol dependence measured with positron emission tomography. *Mol. Psychiatr.* **18**, 916–921 (2013).
11. Kumar, R. N., Chambers, W. A. & Pertwee, R. G. Pharmacological actions and therapeutic uses of cannabis and cannabinoids. *Anaesthesia* **56**, 1059–1068 (2001).
12. Pertwee, R. G. Pharmacological actions of cannabinoids. *Handb. Exp. Pharmacol.* https://doi.org/10.1007/3-540-26573-2_1 (2005).
13. Wick, M. J. et al. Mutations of γ-aminobutyric acid and glycine receptors change alcohol cutoff: evidence for an alcohol receptor? *Proc. Natl Acad. Sci. USA* **95**, 6504–6509 (1998).
14. Burgos, C. F., Munoz, B., Guzman, L. & Aguayo, L. G. Ethanol effects on glycinergic transmission: from molecular pharmacology to behavior responses. *Pharmacol. Res.* **101**, 18–29 (2015).
15. Trudell, J. R., Messing, R. O., Mayfield, J. & Harris, R. A. Alcohol dependence: molecular and behavioral evidence. *Trends Pharmacol. Sci.* **35**, 317–323 (2014).
16. Lynch, J. W., Zhang, Y., Talwar, S. & Estrada-Mondragon, A. Glycine receptor drug discovery. *Adv. Pharmacol.* **79**, 225–253 (2017).
17. Yevenes, G. E. & Zeilhofer, H. U. Allosteric modulation of glycine receptors. *Br. J. Pharmacol.* **164**, 224–236 (2011).
18. Avila, A., Nguyen, L. & Rigo, J. M. Glycine receptors and brain development. *Front. Cell Neurosci.* **7**, 184 (2013).
19. Aguayo, L. G., van Zundert, B., Tapia, J. C., Carrasco, M. A. & Alvarez, F. J. Changes on the properties of glycine receptors during neuronal development. *Brain Res. Rev.* **47**, 33–45 (2004).
20. Zou, G. C. et al. Cannabinoids Rescue cocaine-induced seizures by restoring brain glycine receptor dysfunction. *Cell Rep.* **30**, 4209–4219 (2020).
21. Steiner, H., Bonner, T. I., Zimmer, A. M., Kitai, S. T. & Zimmer, A. Altered gene expression in striatal projection neurons in CB1 cannabinoid receptor knockout mice. *Proc. Natl Acad. Sci. USA* **96**, 5786–5790 (1999).
22. Kishimoto, Y. & Kano, M. Endogenous cannabinoid signaling through the CB1 receptor is essential for cerebellum-dependent discrete motor learning. *J. Neurosci.* **26**, 8829–8837 (2006).
23. Schaefer, N. et al. Disruption of a structurally important extracellular element in the glycine receptor leads to decreased synaptic integration and signaling resulting in severe startle disease. *J. Neurosci.* **37**, 7948–7961 (2017).
24. Crisp, S. J. et al. Glycine receptor autoantibodies disrupt inhibitory neurotransmission. *Brain: a J. Neurol.* **142**, 3398–3410 (2019).
25. Harvey, R. J., Topf, M., Harvey, K. & Rees, M. I. The genetics of hyperekplexia: more than startle! *Trends Genet.* **24**, 439–447 (2008).
26. Jin, S. et al. Brain ethanol metabolism by astrocytic ALDH2 drives the behavioural effects of ethanol intoxication. *Nat. Metab.* **3**, 337–351 (2021).
27. DeSanty, K. P. & Dar, M. S. Cannabinoid-induced motor incoordination through the cerebellar CB1 receptor in mice. *Pharmacol. Biochem. Behav.* **69**, 251–259 (2001).
28. Sanes, J. N. Motor cortex rules for learning and memory. *Curr. Biol.* **10**, R495–R497 (2000).
29. Bullitt, E. Expression of C-Fos-like protein as a marker for neuronal-activity following noxious-stimulation in the rat. *J. Comp. Neurol.* **296**, 517–530 (1990).
30. Armbruster, B. N., Li, X., Pausch, M. H., Herlitze, S. & Roth, B. L. Evolving the lock to fit the key to create a family of G protein-coupled receptors potently activated by an inert ligand. *Proc. Natl Acad. Sci. USA* **104**, 5163–5168 (2007).
31. Schiffmann, S. N. et al. Impaired motor coordination and Purkinje cell excitability in mice lacking calretinin. *PNAS* **96**, 5257–5262 (1999).
32. Shibasaki, K., Ishizaki, Y. & Mandadi, S. Astrocytes express functional TRPV2 ion channels. *Biochem. Biophys. Res. Commun.* **441**, 327–332 (2013).
33. Herkenham, M. et al. Cannabinoid receptor localization in brain. *Proc. Natl Acad. Sci. USA* **87**, 1932–1936 (1990).
34. Arenas, Y. M., Cabrera-Pastor, A., Juciute, N., Mora-Navarro, E. & Felipo, V. Blocking glycine receptors reduces neuroinflammation and restores neurotransmission in cerebellum through ADAM17-TNFR1-NF-κβ pathway. *J. Neuroinflammation* **17**, 269 (2020).
35. Xiong, W. et al. Cannabinoid potentiation of glycine receptors contributes to cannabis-induced analgesia. *Nat. Chem. Biol.* **7**, 296–303 (2011).
36. Xiong, W. et al. Cannabinoids suppress inflammatory and neuropathic pain by targeting α3 glycine receptors. *J. Exp. Med.* **209**, 1121–1134 (2012).
37. Xiong, W. et al. A common molecular basis for exogenous and endogenous cannabinoid potentiation of glycine receptors (April, pg 5200, 2012). *J. Neurosci.* **32**, 12979–12979 (2012).
38. Lu, J. et al. Involvement of glycine receptor α1 subunits in cannabinoid-induced analgesia. *Neuropharmacology* **133**, 224–232 (2018).
39. Wells, M. M. et al. Ensemble-based virtual screening for cannabinoid-like potentiators of the human glycine receptor α1 for the treatment of pain. *J. Med. Chem.* **58**, 2958–2966 (2015).
40. Molnar, E. Motor learning and long-term plasticity of parallel fibre-Purkinje cell synapses require post-synaptic Cdk5/p35. *J. Neurochem.* **131**, 1–3 (2014).
41. Yao, L. et al. Membrane cholesterol dependence of cannabinoid modulation of glycine receptor. *FASEB J.* **34**, 10920–10930 (2020).
42. Zou, G., Xia, J., Han, Q., Liu, D. & Xiong, W. The synthetic cannabinoid dehydroxylcannabidiol restores the function of a major GABAA receptor isoform in a cell model of hyperekplexia. *J. Biol. Chem.* **295**, 138–145 (2020).
43. Scherma, M. et al. Brain activity of anandamide: a rewarding bliss. *Acta Pharmacol. Sin.* **40**, 309–323 (2019).
44. Calapai, F. et al. Cannabinoids, blood–brain barrier, and brain disposition. *Pharmaceutics* https://doi.org/10.3390/pharmaceutics12030265 (2020).
45. Fei, C., Lillico, D. M. E., Hall, B., Rieger, A. M. & Stafford, J. L. Connected component masking accurately identifies the ratio of phagocytosed and cell-bound particles in individual cells by imaging flow cytometry. *Cytom. Part A* **91**, 372–381 (2017).
46. Xue, J. et al. Neutrophil-mediated anticancer drug delivery for suppression of postoperative malignant glioma recurrence. *Nat. Nanotechnol.* **12**, 692–700 (2017).
47. Li, W. et al. BBB pathophysiology-independent delivery of siRNA in traumatic brain injury. *Sci Adv* https://doi.org/10.1126/sciadv.abd6889 (2021).
48. Li, G. et al. Permeability of endothelial and astrocyte cocultures: in vitro blood–brain barrier models for drug delivery studies. *Ann. Biomed. Eng.* **38**, 2499–2511 (2010).
49. Roth, J. G. et al. Advancing models of neural development with biomaterials. *Nat. Rev. Neurosci.* **22**, 593–615 (2021).
50. Dono, L. M. & Currie, P. J. The cannabinoid receptor CB1 inverse agonist AM251 potentiates the anxiogenic activity of urocortin I in the basolateral amygdala. *Neuropharmacology* **62**, 192–199 (2012).
51. Bogdanov, N. N., Poletaeva, I. I. & Popova, N. V. Pentylenetetrazol and strychnine convulsions in brain weight selected mice. *Seizure* **6**, 135–138 (1997).
52. Metrik, J., Gunn, R. L., Jackson, K. M., Sokolovsky, A. W. & Borsari, B. Daily patterns of marijuana and alcohol co-use among individuals with alcohol and cannabis use disorders. *Alcohol Clin. Exp. Res* **42**, 1096–1104 (2018).
53. Wolfe, S. A., Vozella, V. & Roberto, M. The synaptic interactions of alcohol and the endogenous cannabinoid system. *Alcohol Res.* **42**, 03 (2022).
54. Xiong, W. et al. Presynaptic glycine receptors as a potential therapeutic target for hyperekplexia disease. *Nat. Neurosci.* **17**, 232–239 (2014).
55. Dar, M. S. & Mustafa, S. J. Acute ethanol/cannabinoid-induced ataxia and its antagonism by oral/systemic/intracerebellar A1 adenosine receptor antisense in mice. *Brain Res.* **957**, 53–60 (2002).
56. Smith, A. D. & Dar, M. S. Mouse cerebellar nicotinic-cholinergic receptor modulation of δ9-THC ataxia: role of the α4β2 subtype. *Brain Res.* **1115**, 16–25 (2006).
57. Hanig, J. P., Morrison, J. M. Jr. & Krop, S. Ethanol enhancement of blood–brain barrier permeability to catecholamines in chicks. *Eur. J. Pharmacol.* **18**, 79–82 (1972).
58. Pan, W., Barron, M., Hsuchou, H., Tu, H. & Kastin, A. J. Increased leptin permeation across the blood–brain barrier after chronic alcohol ingestion. *Neuropsychopharmacology* **33**, 859–866 (2008).
59. Haorah, J. et al. Ethanol-induced activation of myosin light chain kinase leads to dysfunction of tight junctions and blood–brain barrier compromise. *Alcohol. Clin. Exp. Res.* **29**, 999–1009 (2005).

60. Haorah, J., Knipe, B., Leibhart, J., Ghorpade, A. & Persidsky, Y. Alcohol-induced oxidative stress in brain endothelial cells causes blood–brain barrier dysfunction. *J. Leukoc. Biol.* **78**, 1223–1232 (2005).
61. Lukas, S. E. & Orozco, S. Ethanol increases plasma δ(9)-tetrahydrocannabinol (THC) levels and subjective effects after marihuana smoking in human volunteers. *Drug Alcohol Depend.* **64**, 143–149 (2001).
62. Blazquez, C. et al. Inhibition of striatonigral autophagy as a link between cannabinoid intoxication and impairment of motor coordination. *eLife* **9**, e56811 (2020).
63. Patra, M. et al. Under the influence of alcohol: the effect of ethanol and methanol on lipid bilayers. *Biophys. J.* **90**, 1121–1135 (2006).
64. Goldstein, D. B. Effect of alcohol on cellular membranes. *Ann. Emerg. Med.* **15**, 1013–1018 (1986).
65. Ingolfsson, H. I. & Andersen, O. S. Alcohol's effects on lipid bilayer properties. *Biophys. J.* **101**, 847–855 (2011).
66. Karila, L. et al. Acute and long-term effects of cannabis use: a review. *Curr. Pharm. Des.* **20**, 4112–4118 (2014).
67. Chattipakorn, S. C. & McMahon, L. L. Strychnine-sensitive glycine receptors depress hyperexcitability in rat dentate gyrus. *J. Neurophysiol.* **89**, 1339–1342 (2003).
68. Sink, K. S. et al. Potential anxiogenic effects of cannabinoid CB1 receptor antagonists/inverse agonists in rats: comparisons between AM4113, AM251, and the benzodiazepine inverse agonist FG-7142. *Eur. Neuropsychopharmacol.* **20**, 112–122 (2010).
69. Zhao, Q. C. et al. HDAC3 inhibition prevents blood–brain barrier permeability through Nrf2 activation in type 2 diabetes male mice. *J. Neuroinflamm* **16**, 103 (2019).
70. Wilkinson, S. M., Price, J. & Kassiou, M. Improved accessibility to the desoxy analogues of δ(9)-tetrahydrocannabinol and cannabidiol. *Tetrahedron Lett.* **54**, 52–54 (2013).

Acknowledgements

We thank T. Pan for the synthesis of THC, THC–Cy7 and DDT. We thank G.E. Homanics (University of Pittsburgh) for providing the GlyRα1^{S296A} mice. This work was supported by National Key R&D Program of China (2021YFA0804900, W.X.), National Natural Science Foundation of China (grants 91849206, 91649121, 91942315, 92049304, 32121002, 32225020 to W.X.; 81901157 to G.Z.), the Strategic Priority Research Program of the Chinese Academy of Sciences (grant XDB39050000, W.X.), Key Research Program of Frontier Science (CAS, grant ZDBS-LY-SM002, W.X.), CAS Interdisciplinary Innovation Team (JCTD-2018-20, W.X.), CAS Project for Young Scientists in Basic Research (YSBR-013, W.X.), the Fundamental Research Funds for the Central Universities, the Major Program of Development Foundation of Hefei Center for Physical Science and Technology (2017FXZY006, W.X.) and Users with Excellence Program/ Project of Hefei Science Center CAS (2019HSC-UE006, W.X.), USTC Research Funds of the Double First-Class Initiative (YD9100002001, W.X.) and China Postdoctoral Science Foundation (2020TQ0314, G.Z.).

Author contributions

W.X. initiated, designed and supervised the project; G.Z., C.M. and H.L. conducted electrophysiological recordings. G.Z., J.X. and X.Z. conducted behavior tests; G.Z. and D.X. conducted immunohistochemistry; Y.Y., Q.G. and J.X. conducted the BBB experiments. G.Z. and J.X. conducted the quantitative flow cytometry, in vivo small animal imaging and HPLC–MS experiments. G.Z. and W.X. analyzed data with assistance of T.X, Z.Z. and Y.Z. L.Z. contributed to experimental design, data interpretation and analysis. W.X. and G.Z wrote the manuscript.

Competing interests

The authors declare no competing interests.

Additional information

Extended data is available for this paper at https://doi.org/10.1038/s42255-022-00633-6.

Supplementary information The online version contains supplementary material available at https://doi.org/10.1038/s42255-022-00633-6.

Correspondence and requests for materials should be addressed to Wei Xiong.

Peer review information *Nature Metabolism* thanks the anonymous reviewers for their contribution to the peer review of this work. Ashley Castellanos-Jankiewicz, in collaboration with the *Nature Metabolism* team.

Reprints and permissions information is available at www.nature.com/reprints.

Publisher's note Springer Nature remains neutral with regard to jurisdictional claims in published maps and institutional affiliations.

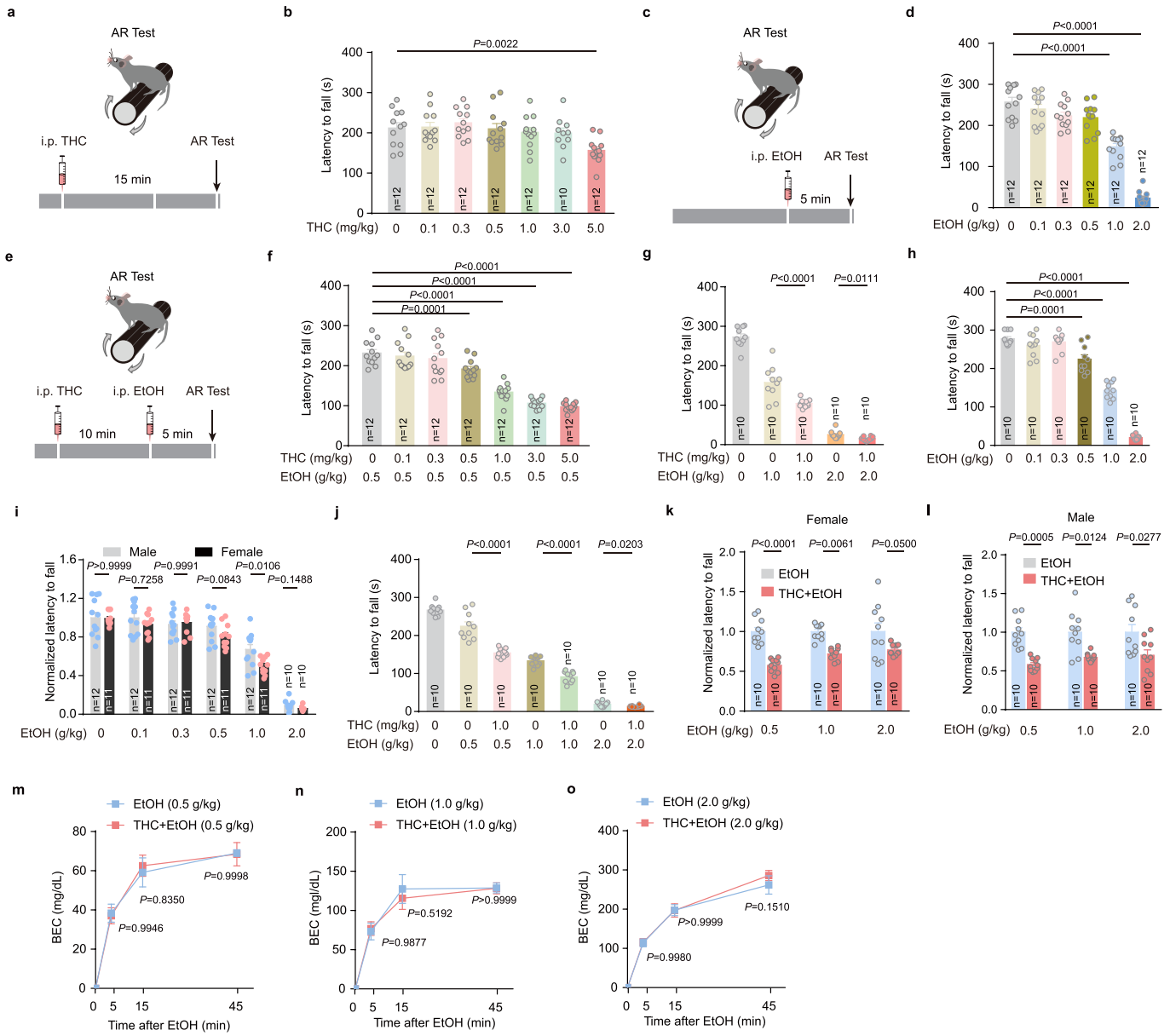

Extended Data Fig. 1 | Effects of THC and ethanol on motor coordination and the BEC in mice, Related to Fig. 1. a, Schematic showing the timeline of drug administration and AR procedure. **b**, Effects of THC (i.p., 0.1, 0.3, 0.5, 1.0, 3.0 and 5.0 mg/kg) on AR latency of mice. **c**, Schematic showing the timeline of drug administration and AR procedure. **d**, Effects of ethanol (i.p., 0.1, 0.3, 0.5, 1.0 and 2.0 g/kg) on AR latency of mice. **e**, Schematic showing the timeline of drug administration and AR procedure. **f**, Effects of THC and ethanol in combination on AR latency of mice. **g**, Effects of ethanol (i.p., 1.0 and 2.0 g/kg) alone or in combination with THC (i.p., 1.0 mg/kg) on AR latency of mice. **h**, Effects of ethanol on AR latency of female mice. **i**, Compare of effects of ethanol on AR latency between male and female mice. Each data were normalized to its control group. **j**, Effects of ethanol (i.p., 0.5, 1.0 and 2.0 g/kg) alone or in combination with THC (i.p., 1.0 mg/kg) on AR latency in female mice. **k**,**l**, Normalized AR latency of female (**k**) and male (**l**) mice receiving THC (i.p., 1.0 mg/kg) and ethanol (i.p., 0.5, 1.0 and 2.0 g/kg) in combination. Each data were normalized to the related ethanol alone group. **m-o**, BEC of mice treated with i.p. ethanol at 0.5 g/kg (**m**), 1.0 g/kg (**n**) or 2.0 g/kg (**o**) alone with or without i.p. THC (1.0 mg/kg). n = 3 mice per group. Values are represented as means ± s.e.m., *n* per group. Exact *P* values are shown. Statistical differences were determined by a one-way ANOVA followed by Tukey's post hoc multiple-comparison test (**b**, **d**, **f**-**h**, **j**) or a two-way ANOVA followed by Tukey's post hoc multiple-comparison test (**i**, **k**, **l**, **m**-**o**).

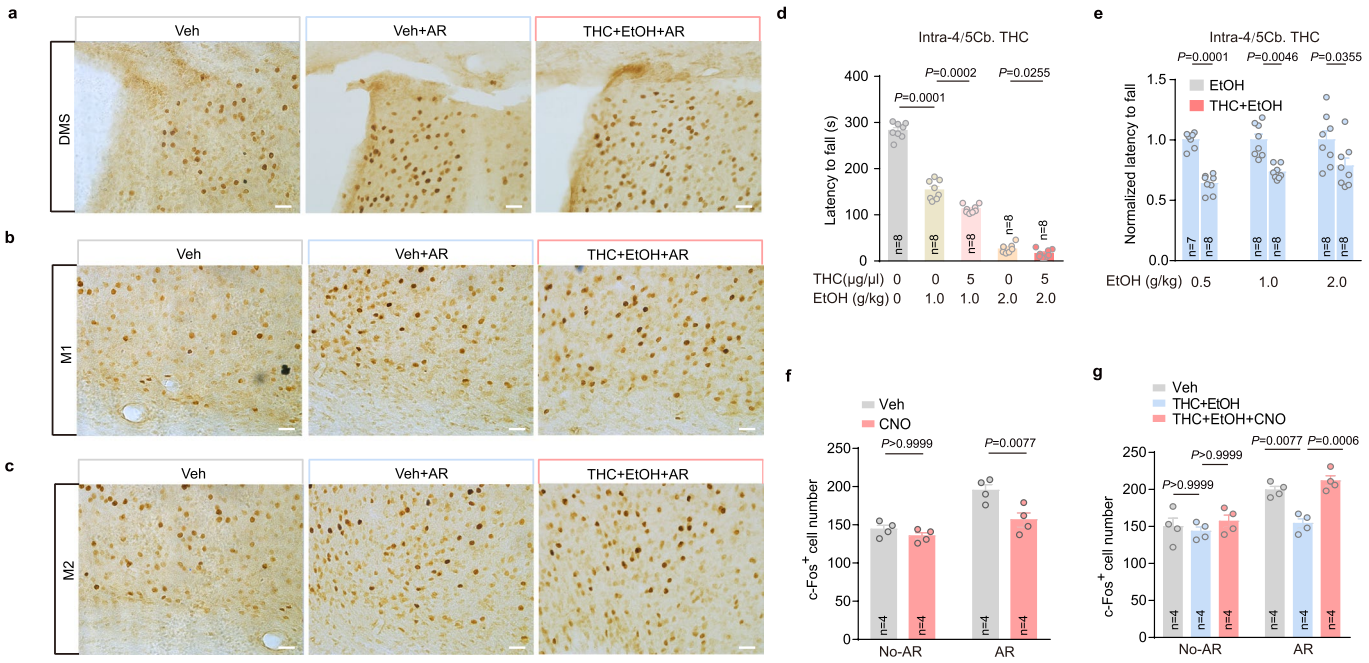

Extended Data Fig. 2 | The synergistic effect of THC and various doses of systemic ethanol on c-Fos immunohistochemistry in various brain regions and motor coordination, Related to Fig. 1. a-c Representative images of immunohistochemistry c-Fos positive neurons in DMS, M1 and M2 of mice treated with Veh, Veh + AR or THC + ethanol + AR. Scale bar, 25 μm. Veh: vehicle, AR: accelerating rotarod. **d**, Effects of ethanol alone or in combination with THC (intra-4/5Cb., 5 μg/μl) on AR latency of mice. **e**, Normalized AR latency of mice receiving THC (intra-4/5Cb., 5 μg/μl) and ethanol in combination. Each data were normalized to the ethanol group with the same dose of ethanol. **f**, Effects of CNO (i.p., 1.0 mg/kg) on the number of c-Fos positive neurons in cerebellar 4/5Cb of mice transfected with AAV2/9-hSyn-hM4Di-mCitrine with or without AR tests. **g**, Effects of THC (i.p., 1.0 mg/kg) + ethanol (i.p., 0.5 g/kg), CNO (i.p., 1.0 mg/kg), or their combination on the number of c-Fos positive neurons in cerebellar 4/5Cb of mice expressing AAV2/9-hSyn-hM3Dq-mCitrine with or without AR tests. Values are represented as means ± s.e.m., *n* per group. Exact *P* values are shown. Statistical differences were determined by a one-way ANOVA followed by Tukey's post hoc multiple-comparison test (**d**) or a two-way ANOVA followed by Tukey's post hoc multiple-comparison test (**e**-**g**).

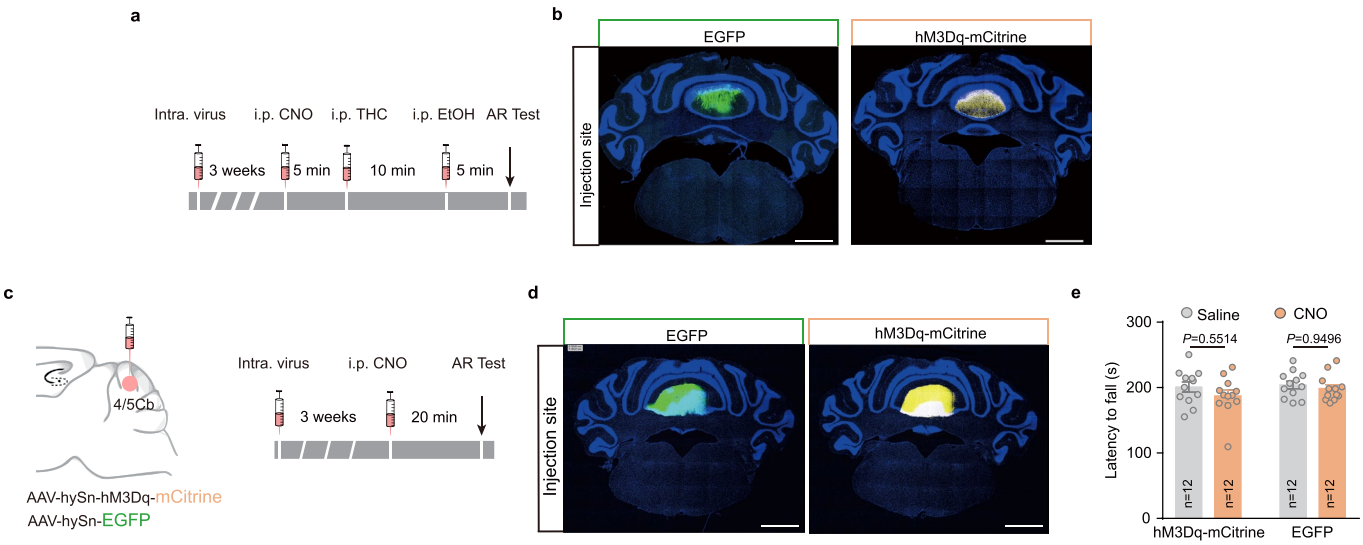

Extended Data Fig. 3 | Effects of chemogenetic activation of 4/5Cb on motor coordination in mice, Related to Fig. 1. a, Schematic showing the timeline of chemogenetic experimental procedure. AAV2/9-hSyn-hM3Dq-mCitrine or the AAV2/9-hSyn-EGFP was injected into the 4/5Cb of mice. **b**, Representative images showing the EGFP or mCitrine signals in the injection sites of the 4/5Cb of mice. Scale bar, 1 mm. **c**, Schematic showing virus injection and chemogenetic experimental procedure. AAV2/9-hSyn-hM3Dq-mCitrine or the AAV2/9-hSyn-EGFP was injected into the 4/5Cb of mice. **d**, Representative images showing the EGFP or mCitrine signals in the injection sites of the 4/5Cb of mice. Scale bar, 1 mm. **e**, Effects of CNO (i.p., 1.0 mg/kg) on AR latency of mice expressing hM3Dq or EGFP as a control in the 4/5Cb. Values are represented as means ± s.e.m., *n* per group. Statistical differences were determined by a two-way ANOVA followed by Tukey's post hoc multiple-comparison test.

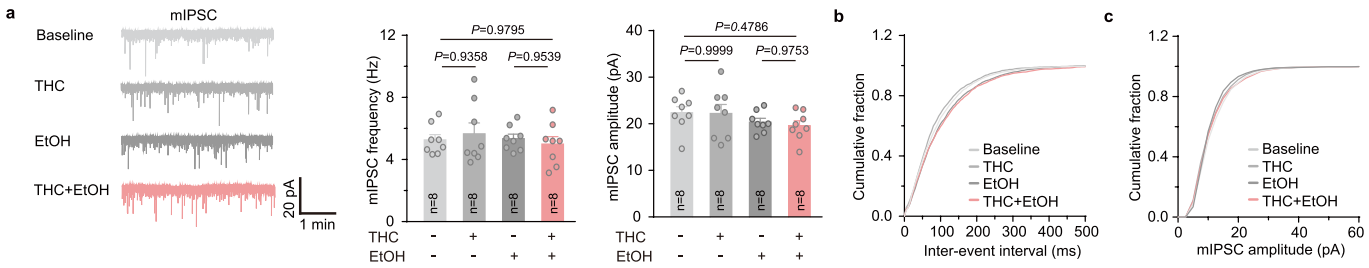

Extended Data Fig. 4 | Effects of THC and ethanol combination on mIPSCs of PCs, Related to Fig. 2. a, Trace records, average frequency and amplitude of GABAergic mIPSCs of PCs in 4/5Cb slices of mice. The neurons recorded were treated with THC (100 nM, 5 min) and ethanol (20 mM, 5 min), either alone or in combination. **b**,**c**, Cumulative probability plot for the inter-event interval (**b**) and amplitudes (**c**) for GABAergic mIPSCs of PCs in 4/5Cb slices of mice. Values are represented as means ± s.e.m., *n* per group. Statistical differences were determined by a one-way ANOVA followed by Tukey's post hoc multiple-comparison test.

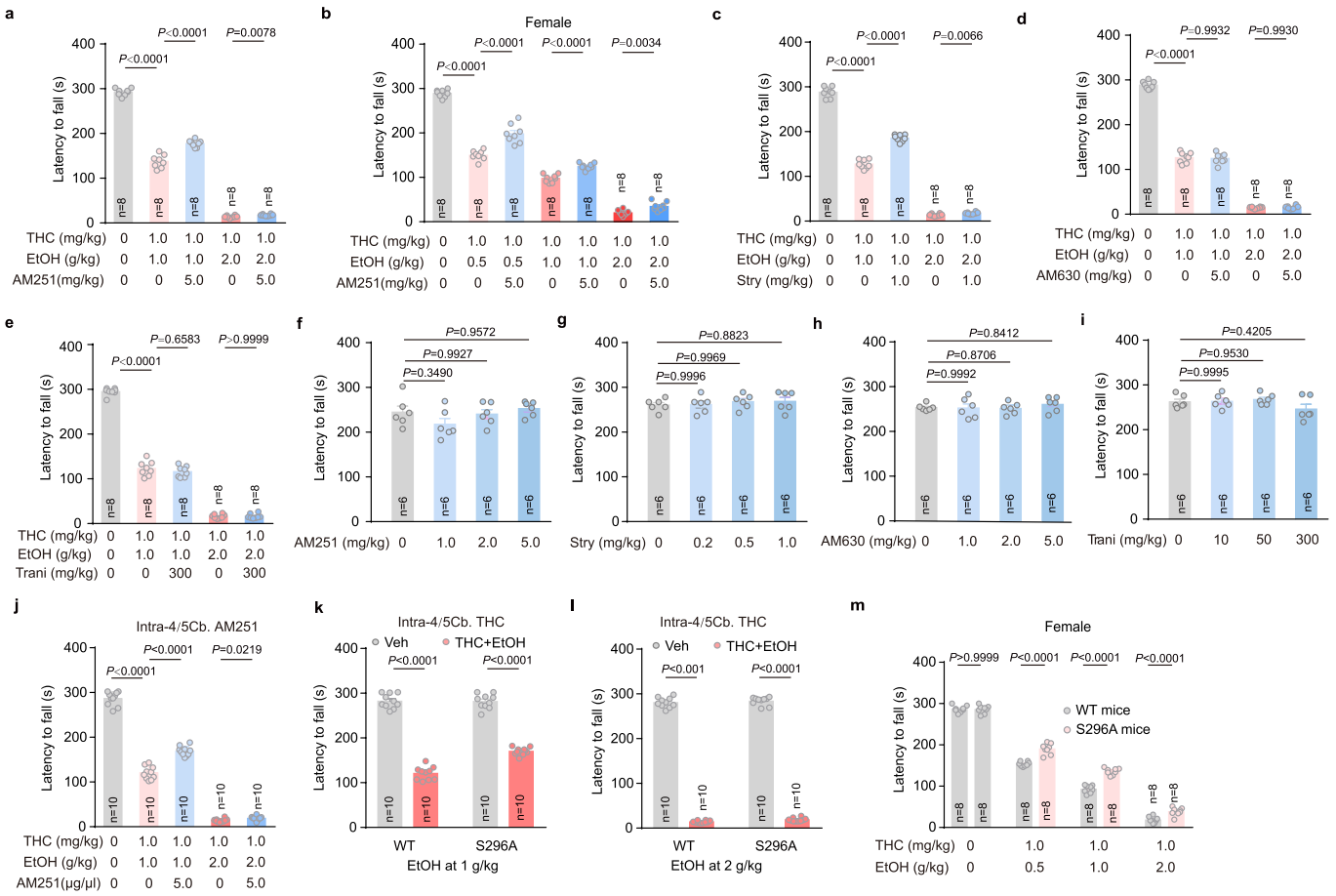

Extended Data Fig. 5 | Effects of various antagonists on SETEM and motor coordination in mice, Related to Fig. 3. a,**b**, Effects of AM251 (i.p., 5.0 mg/kg) on the SETEM caused by THC (i.p., 1.0 mg/kg) and ethanol (i.p., 0.5, 1.0 and 2.0 g/kg) combination in male (**a**) and female (**b**) mice. **c-e**, Effects of strychnine (i.p., 1.0 mg/kg) (**c**), AM630 (i.p., 5.0 mg/kg) (**d**) and tranilast (i.p., 300 mg/kg) (**e**) on the SETEM caused by THC (i.p., 1.0 mg/kg) and ethanol (i.p., 1.0 and 2.0 g/kg) combination in mice. Stry: strychnine; Trani: Tranilast. **f-i**, Effects of AM251(**f**), strychnine (**g**), AM630(**h**) and tranilast (**i**) on AR latency of mice. **j**, Effects of AM251 (intra-4/5Cb., 5 μg /μl) on the SETEM caused by THC (i.p., 1.0 mg/kg) and ethanol (i.p., 1.0 and 2.0 g/kg) combination in mice. **k**, Effects of THC (intra-4/5Cb., 5 μg/μl) and ethanol (i.p., 1.0 g/kg) combination on AR latency in GlyRα1^{WT} and GlyRα1^{S296A} mice. **l**, Effects of THC (intra-4/5Cb., 5 μg/μl) and ethanol (i.p., 2.0 g/kg) combination on AR latency in GlyRα1^{WT} and GlyRα1^{S296A} mice. **m**, The AR latency of GlyRα1^{WT} and GlyRα1^{S296A} female mice receiving THC (i.p., 1.0 mg/kg) and ethanol (i.p., 0.5, 1.0 and 2.0 g/kg) combination. Values are represented as means ± s.e.m., *n* per group. Exact *P* values are shown. Statistical differences were determined by a one-way ANOVA followed by Tukey's post hoc multiple-comparison test (**a-j**) or a two-way ANOVA followed by Tukey's post hoc multiple-comparison test (**k**-**m**).

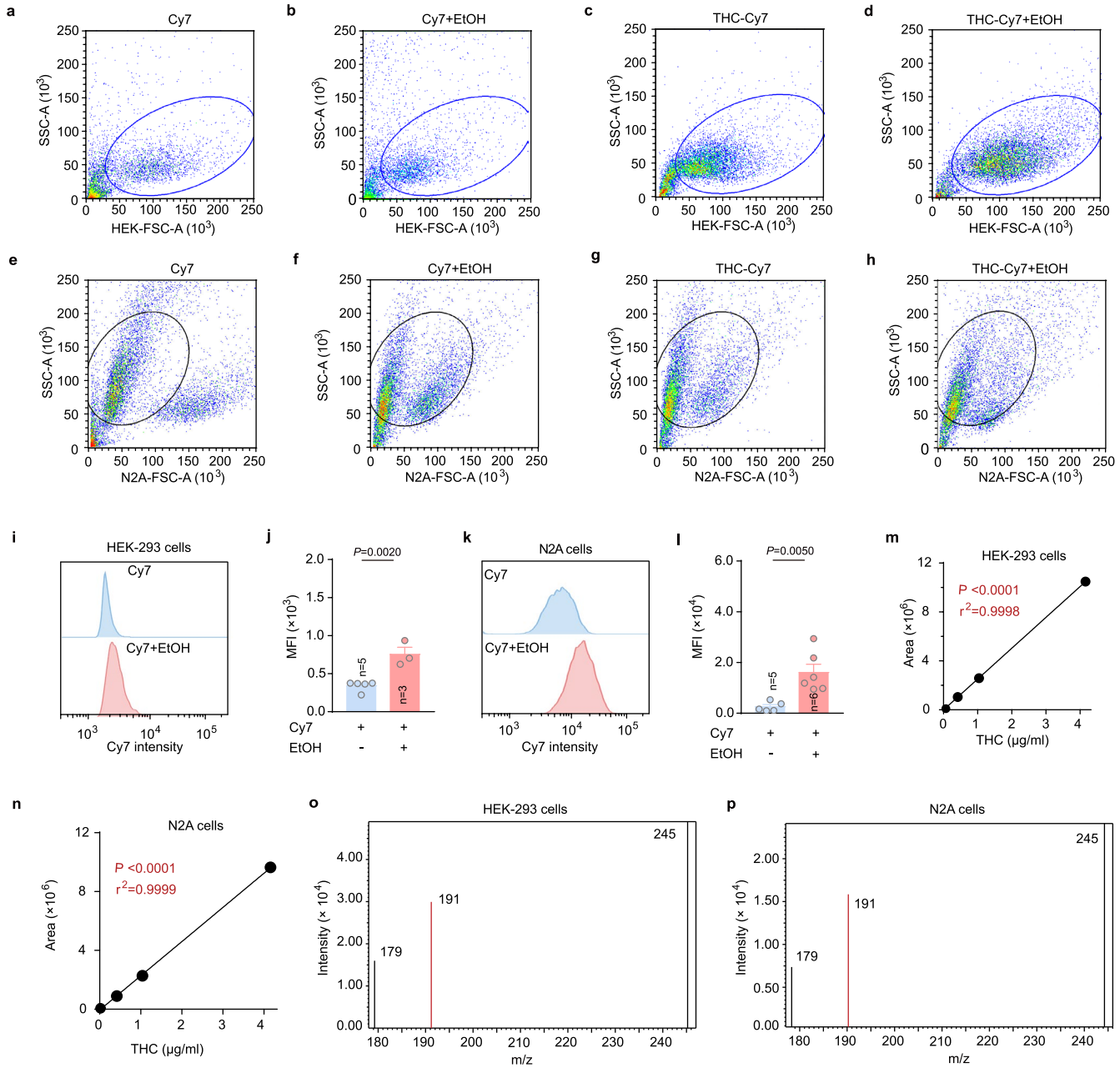

Extended Data Fig. 6 | Effects of ethanol on Cy7 level in HEK-293 cells and N2A cells measured by standard flow cytometry, Related to Fig. 6. a-d, Gating strategy to obtain HEK-293 cells with similar size (FSC-A) and granularity (SSC-A). The HEK-293 cells have been incubated with Cy7 (**a**), Cy7 + ethanol (**b**), THC-Cy7 (**c**) and THC-Cy7 + ethanol (**d**) for 60 min, respectively. Cy7 at 10 μM, THC-Cy7 at 10 μM and ethanol at 20 mM were used in this experiment. FSC-A: Forward Scatter Area; SSC-A: Side Scatter Area. **e-h**, Gating strategy to obtain N2A cells with similar size (FSC-A) and granularity (SSC-A). The N2A cells have been incubated with Cy7 (**e**), Cy7 + ethanol (**f**), THC-Cy7 (**g**) and THC-Cy7 + ethanol (**h**) for 60 min, respectively. **i**,**j** Histograms (**i**) and bar graph (**j**) of MFI (Median Fluorescence Intensity) obtained from standard flow cytometry analysis of HEK-293 cells treated with Cy7 or Cy7 plus ethanol in combination. **k**,**l** Histograms (**k**) and bar graph (**l**) of MFI obtained from standard flow cytometry analysis of N2A cells treated with Cy7 or Cy7 plus ethanol in combination. **m**, HPLC calibration curve of HEK-293 cell buffer spiked with known amounts of THC. The calibration curve: y = 2180.40x − 1662.02. **n**, HPLC calibration curve of N2A cell buffer spiked with known amounts of THC. The calibration curve: y = 2495.71x + 418.599. **o**,**p** Representative mass spectra of THC obtained from HEK-293 cell (**o**) and N2A cell (**p**) buffer. Values are represented as means ± s.e.m., *n* per group. Exact *P* values are shown. Statistical differences were determined by a a two-sided unpaired t-test (**j** and **l**) or a linear regression test (**m** and **n**).

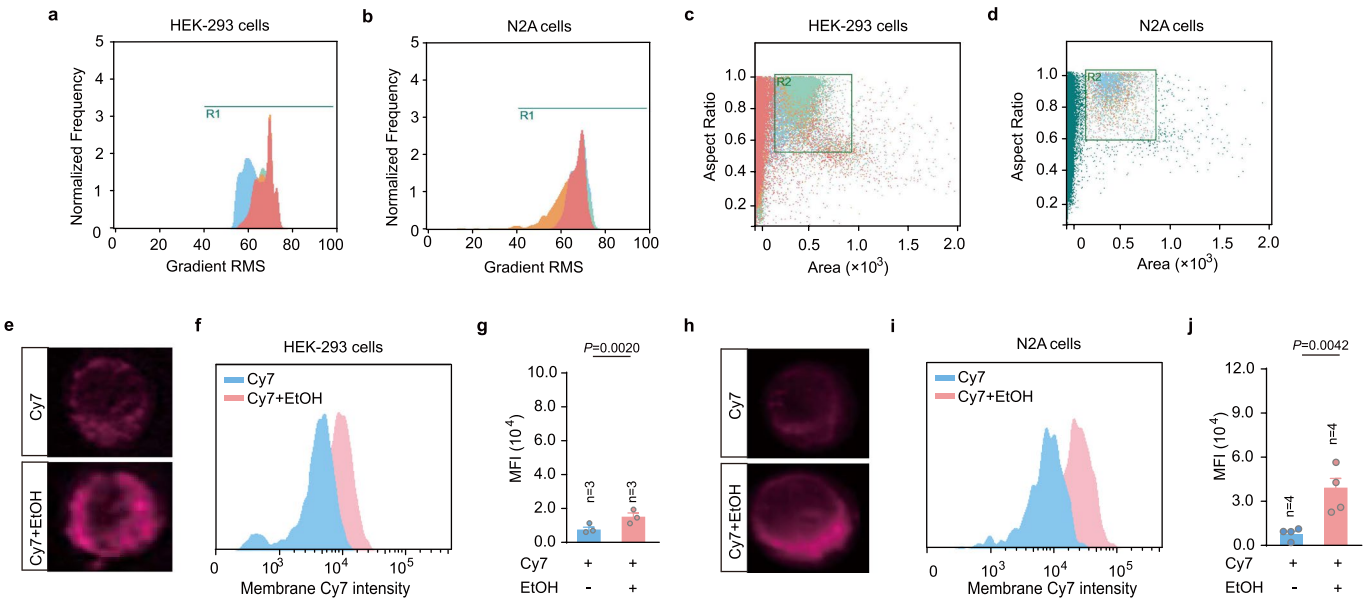

Extended Data Fig. 7 | Effects of ethanol on Cy7 level in HEK-293 cells and N2A cells measured by imaging flow cytometr, Related to Fig. 6. a, **b** Representative histogram used to discriminate between unfocused and focused images of HEK-293 cells (**a**) and N2A cells (**b**) incubated with Cy7, Cy7 + ethanol, THC-Cy7 and THC-Cy7 + ethanol. Cy7 at 10 μM, THC-Cy7 at 10 μM and ethanol at 20 mM were used. These experiments were done using the standard IDEAS® software platform. Upon this image, Gradient RMS values between 40–100 (R1: Region 1) were included for further analysis. Gradient RMS: Root Mean Square. **c**,**d** Representative graph of area versus aspect ratio used to gating focused images of HEK-293 cells (**c**) and N2A cells (**d**). Cells in the frame (R2: Region 2) were used for further membrane intensity analysis. Area: size of the focused cells; Aspect ratio: the minor axis divided by the major axis of the focused cells. **e-g**, Representative cell images (**e**), histograms (**f**) and bar graphs (**g**) of MFI obtained from IFC (Imaging Flow Cytometry) of HEK-293 cells treated with Cy7 or Cy7 and ethanol in combination. **h-j**, Representative cell images (**h**), histograms (**i**) and bar graphs (**j**) of MFI obtained from IFC of N2A cells treated with Cy7 or Cy7 and ethanol in combination. Values are represented as means ± s.e.m., *n* per group. Exact *P* values are shown. Statistical differences were determined by a two-sided unpaired *t*-test.

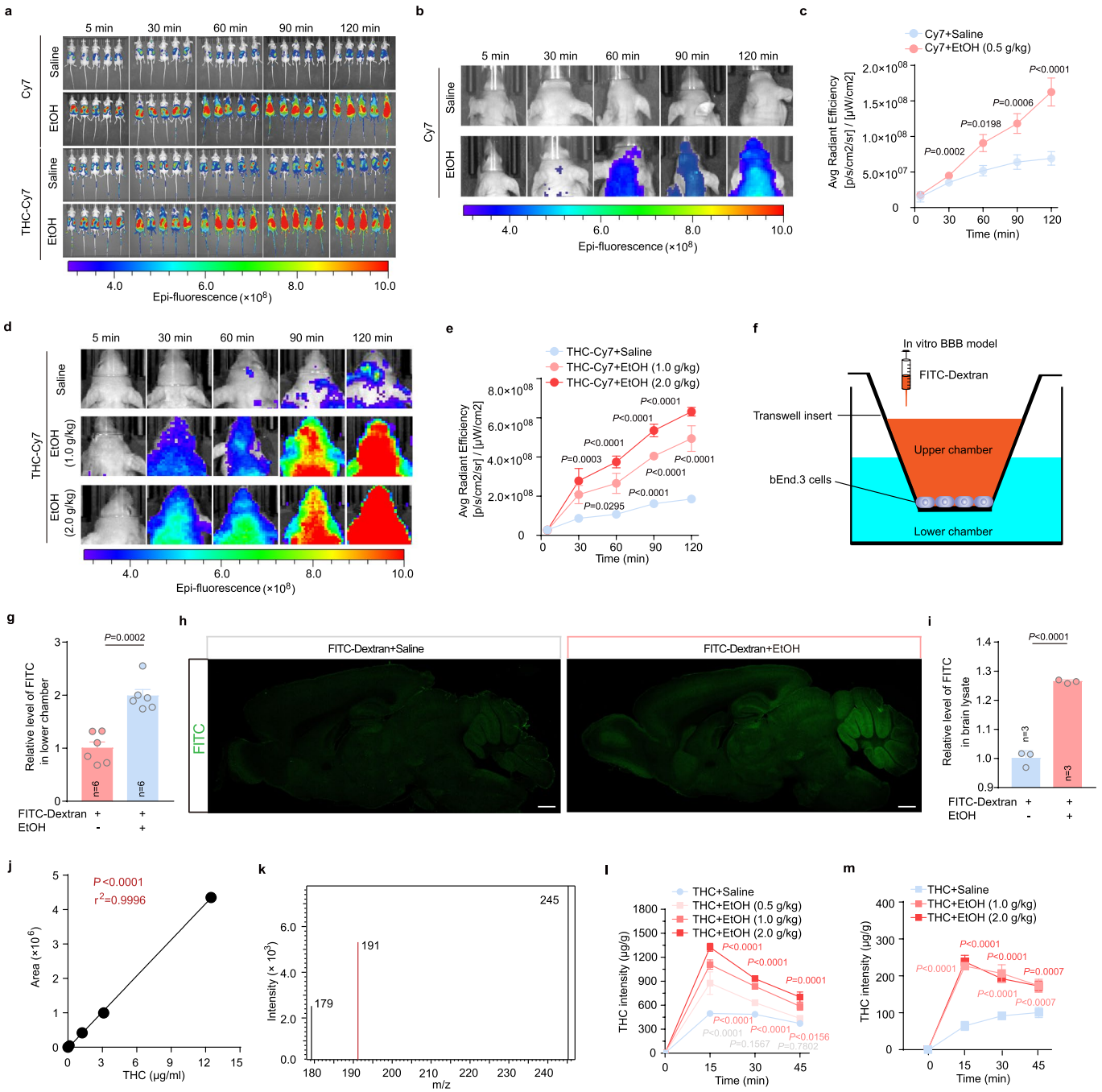

Extended Data Fig. 8 | Effects of various doses of ethanol on plasma and brain intensity of THC and BBB permeability. Related to Fig. 7. a, Whole body fluorescence imaging of mice treated with Cy7/Cy7-THC (i.p., 10 mg/kg) or Cy7/Cy7-THC (i.p., 10 mg/kg) and ethanol (i.p., 0.5 g/kg) in combination. **b**, Representative fluorescence images of mice treated with Cy7 alone or Cy7 with ethanol in combination. **c**, Brain fluorescence intensity of Cy7. n = 5 mice per group. **d**, Representative fluorescence images of mice treated with THC-Cy7 or THC-Cy7 with ethanol in combination. **e**, Brain fluorescence intensity of THC-Cy7. n = 5 mice per group. **f**, Schematic illustration of the *in vitro* BBB model. **g**, Relative level of FITC-Dextran (1.0 mg/ml, 1 h) crossing endothelial monolayer with or without ethanol (20 mM, 5 min) treatment. **h**,**i**, Representative images (**h**) and quantitative analysis (**i**) of FITC signal in the brain of mice treated with FITC-Dextran (i.p., 50 mg/kg, 1 h) with or without ethanol (i.p., 0.5 g/kg, 5 min) administration. Scale bars: 1 mm. **j**, Calibration curve of plasma spiked with known amounts of THC. The calibration curve: y = 889.307x – 1295.26. **k**, Representative mass spectra of THC obtained from plasma of C57BL/6 J mice administrated with THC (i.p., 10 mg/kg). **l**,**m** Quantitative analysis of plasma (**l**) and cerebellar (**m**) THC intensity in mice treated with THC or THC and ethanol in combination. n = 3 mice per group. Values are represented as means ± s.e.m., *n* per group. Exact *P* values are shown. Statistical differences were determined by a two-sided unpaired *t*-test (**g** and **i**) or a two-way ANOVA followed by Tukey's post hoc multiple-comparison test (**c**, **e**, **l** and **m**) or a linear regression test (**j**).

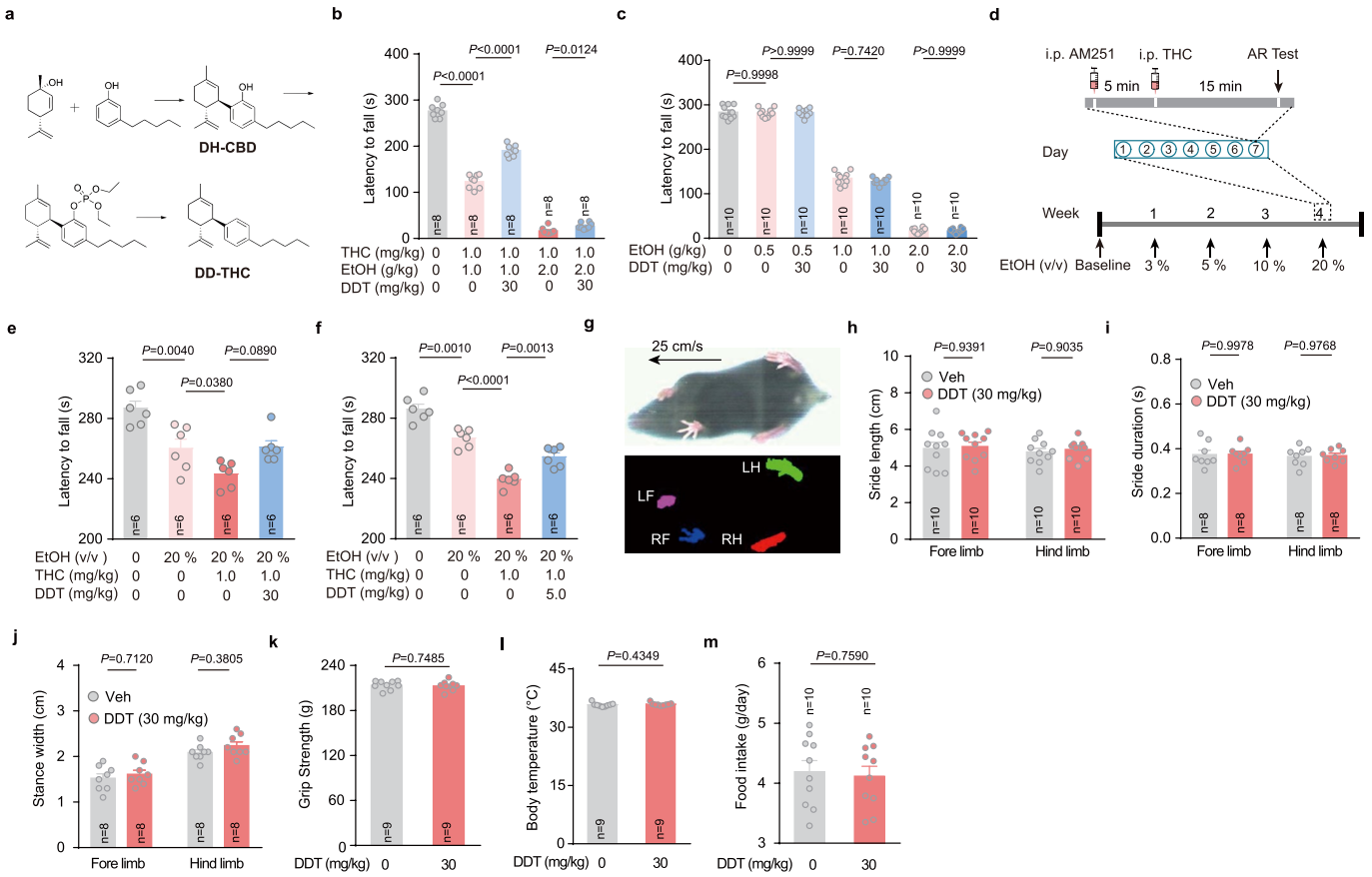

Extended Data Fig. 9 | Effects of DDT on acute and chronic ethanol exposure associated SETEM and ethanol-induced motor incoordination, Related to Fig. 8. **a**, Schematic illustration of synthesis of di-desoxy-THC (DDT). **b**, AR latency of mice receiving THC (i.p., 1.0 mg/kg), ethanol (i.p., 1.0 and 2.0 g/kg), DDT (i.p., 30 mg/kg), or their combination. **c**, Effects of DDT (i.p., 30 mg/kg) on motor incoordination caused by various doses of ethanol. **d**, Schematic illustration of the CEE. **e**, The effects of THC and DDT on the CEE-induced motor incoordination. **f**, The effects of THC and AM251 on the CEE-induced motor incoordination. **g**, Representative images showing a mouse walking on treadmill and its paw prints detected from a video underneath the treadmill. LF: left forelimb; RF: right forelimb; LH: left hindlimb; RH: right hindlimb. **h-j**, Effects of DDT (i.p., 30 mg/kg, 20 min before tests) on the stride length (**h**), stride duration (**i**) and stance width (**j**) of mice in the gait test. **k-m**, Effects of DDT (i.p., 30 mg/kg) on grip strength (**k**), body temperature (**l**) and food intake (**m**) of mice in the grip test. Values are represented as means ± s.e.m., *n* per group. Exact *P* values are shown. Statistical differences were determined by a one-way ANOVA followed by Tukey's post hoc multiple-comparison test (**b**, **c**, **e** and **f**) or a two-way ANOVA followed by Tukey's post hoc multiple-comparison test (**h**-**j**) or a two-sided unpaired *t*-tests (**k**-**m**).

nature research

Corresponding author(s): Wei Xiong

Last updated by author(s): Aug 3, 2022

Reporting Summary

Nature Research wishes to improve the reproducibility of the work that we publish. This form provides structure for consistency and transparency in reporting. For further information on Nature Research policies, see our Editorial Policies and the Editorial Policy Checklist.

Statistics

For all statistical analyses, confirm that the following items are present in the figure legend, table legend, main text, or Methods section.

n/a	Confirmed	
☐	☒	The exact sample size (*n*) for each experimental group/condition, given as a discrete number and unit of measurement
☐	☒	A statement on whether measurements were taken from distinct samples or whether the same sample was measured repeatedly
☐	☒	The statistical test(s) used AND whether they are one- or two-sided *Only common tests should be described solely by name; describe more complex techniques in the Methods section.*
☐	☒	A description of all covariates tested
☐	☒	A description of any assumptions or corrections, such as tests of normality and adjustment for multiple comparisons
☐	☒	A full description of the statistical parameters including central tendency (e.g. means) or other basic estimates (e.g. regression coefficient) AND variation (e.g. standard deviation) or associated estimates of uncertainty (e.g. confidence intervals)
☐	☒	For null hypothesis testing, the test statistic (e.g. *F*, *t*, *r*) with confidence intervals, effect sizes, degrees of freedom and *P* value noted *Give P values as exact values whenever suitable.*
☒	☐	For Bayesian analysis, information on the choice of priors and Markov chain Monte Carlo settings
☒	☐	For hierarchical and complex designs, identification of the appropriate level for tests and full reporting of outcomes
☒	☐	Estimates of effect sizes (e.g. Cohen's *d*, Pearson's *r*), indicating how they were calculated

Our web collection on statistics for biologists contains articles on many of the points above.

Software and code

Policy information about availability of computer code

Data collection	The patch-clamp recording results were collected by Axon 200B and 700B. The ELISA results were collected by Varioskan LUX multi-mode microplate reader (ThermoFisher Scientific, Waltham, MA). The rotarod test results were collected by rotarod system (XR1514, Xinruan, Shanghai, China). The elevated plus maze test results were collected by Elevated Plus Maze (EPM) apparatus (40142, Ugo basile). The startle reflex test results were collected by Med Associates Startle Reflex System (Med Associates Inc.). The immunohistochemistry results were collected by IX73 Inverted microscopes (Olympus) and Zeiss LSM880 confocal fluorescence microscope (Zeiss, USA, San Diego, CA). The Standard flow cytometry results were collected by BD FACSDiva Version 6 Software system (BD Biosciences). The Imaging flow cytometry was collected by the IDEAS®6.2 software. The Live animal imaging were collected by Living Image 2.5 software (PerkinElmer). The HPLC-MS results were collected by Shimadzu LC-20AD series system. The gait was collected with DigiGait® Version 16 software.
Data analysis	The patch-clamp recording data were analyzed by pClamp 10.4 software and GraphPad Prism 8.0. The ELISA results were analyzed by GraphPad Prism 8.0. The immunohistochemistry data were analyzed by Image J software (National Institutes of Health, NIH. https://imagej.nih.gov/ij/). All behavioral results were analyzed by video tracking software (Version 6.0; ANY MAZE) and GraphPad Prism 8. The Standard flow cytometry results were analyzed by FlowJo v10 software and IDEAS® software . The Live animal imaging were analyzed by GraphPad Prism 8.

For manuscripts utilizing custom algorithms or software that are central to the research but not yet described in published literature, software must be made available to editors and reviewers. We strongly encourage code deposition in a community repository (e.g. GitHub). See the Nature Research guidelines for submitting code & software for further information.

Data

Policy information about availability of data

All manuscripts must include a data availability statement. This statement should provide the following information, where applicable:

- Accession codes, unique identifiers, or web links for publicly available datasets
- A list of figures that have associated raw data
- A description of any restrictions on data availability

Source data are provided with this paper.

Field-specific reporting

Please select the one below that is the best fit for your research. If you are not sure, read the appropriate sections before making your selection.

☒ Life sciences ☐ Behavioural & social sciences ☐ Ecological, evolutionary & environmental sciences

For a reference copy of the document with all sections, see nature.com/documents/nr-reporting-summary-flat.pdf

Life sciences study design

All studies must disclose on these points even when the disclosure is negative.

Sample size	No statistical methods were used to predetermine sample size. The sample sizes were selected based on our prior studies that confirm to the standard in the field and assure statistically meaningful differences and repeatability of the results (Zou et al.,Cell reports 2020; Zhu et al., Nature methods 2021; Zhu et al., Cell 2018)
Data exclusions	No data was excluded from the analysis.
Replication	All data collected in this project are presented in this paper including any replication.
Randomization	The samples and mice were randomly allocated to different conditions.
Blinding	For transgenic mice experiments, the investigators were not blinded to group allocation because investigators needed to perform patch-clamp recording and behavioral test. For other experiments including HPLC-MS and flow cytometry , investigators were blinded to group allocation during sample collection and data analysis.

Reporting for specific materials, systems and methods

We require information from authors about some types of materials, experimental systems and methods used in many studies. Here, indicate whether each material, system or method listed is relevant to your study. If you are not sure if a list item applies to your research, read the appropriate section before selecting a response.

Materials & experimental systems

n/a	Involved in the study
☐	☒ Antibodies
☐	☒ Eukaryotic cell lines
☒	☐ Palaeontology and archaeology
☐	☒ Animals and other organisms
☒	☐ Human research participants
☒	☐ Clinical data
☒	☐ Dual use research of concern

Methods

n/a	Involved in the study
☒	☐ ChIP-seq
☐	☒ Flow cytometry
☒	☐ MRI-based neuroimaging

Antibodies

Antibodies used	Rabbit anti-c-Fos (Abcam, ab209794); Goat anti-rabbit IgG (Vector Laboratories, PK-6101); anti-cAMP antibody (Direct cAMP ELISA Kit (Abcam #ab133051))
Validation	All antibodies used in this study are commercially available and have been validated by the manufacture as follows: Rabbit anti-c-Fos (Abcam, ab209794); https://www.abcam.com/c-fos-antibody-ab209794.html Goat anti-rabbit IgG (Vector Laboratories, PK-6101) https://www.biocompare.com/25138-Assay-Kit/10540910-VECTASTAIN-174-Elite-ABC-Peroxidase-Kit/

Cyclic AMP Complete Antibody (Direct cAMP ELISA Kit (Abcam #ab133051))
https://www.abcam.com/ps/products/133/ab133051/documents/ab133051%20-%20Cyclic%20AMP%20Complete%20ELSIA%20Kit%20v3%20(website).pdf

Eukaryotic cell lines

Policy information about cell lines

Cell line source(s)	HEK-293 cells (ATCC); N2A cells (ATCC); bEnd.3 cells (ATCC);
Authentication	All the cell lines were authenticated by qPCR.
Mycoplasma contamination	All the cell lines were not tested for mycoplasma contamination.
Commonly misidentified lines (See ICLAC register)	No commonly misidentified cell lines were used in this study.

Animals and other organisms

Policy information about studies involving animals; ARRIVE guidelines recommended for reporting animal research

Laboratory animals	Wild-type C57BL/6J (male and female, 8 weeks old) and male BALB/c Nude mice (8 weeks old) were obtained from Vital River Laboratory Animal Technology Co., Ltd. (Beijing, China). The male GlyRα1S296A mice (8 weeks old) were obtained from Li Zhang (National Institute on Alcohol Abused and Alcoholism, NIH). All mice were bred and housed under a specific-pathogen-free conditions with 12-h dark/light cycle under 21±1°C temperature and 55–60% humidity and provided ad libitum access to water and food.
Wild animals	No wild animals were used in this study.
Field-collected samples	No field-collected samples were used in this study.
Ethics oversight	All animal procedures were approved by and performed in accordance with the guidelines of the Institutional Animal Use and Care Committee of University of Science & Technology of China.

Note that full information on the approval of the study protocol must also be provided in the manuscript.

Flow Cytometry

Plots

Confirm that:

☒ The axis labels state the marker and fluorochrome used (e.g. CD4-FITC).

☒ The axis scales are clearly visible. Include numbers along axes only for bottom left plot of group (a 'group' is an analysis of identical markers).

☒ All plots are contour plots with outliers or pseudocolor plots.

☒ A numerical value for number of cells or percentage (with statistics) is provided.

Methodology

Sample preparation	HEK-293 and N2A cells were pre-incubated by THC-Cy7.
Instrument	BD FACSDiva Version 6 Software system (BD Biosciences) for Standard flow cytometry; ImageStream Mark II Imaging Flow Cytometry (Amnis, Merck Millipore) for imaging flow cytometry.
Software	FlowJo v10 software for Standard flow cytometry; INSOIRETM software for imaging flow cytometry.
Cell population abundance	At least 5000 events were recorded for each sample during Flow Cytometry analysis.
Gating strategy	For Standard flow cytometry, cells were gated based on FSC-A versus SSC-A parameters and these samples were chosen for fluorescence-activated cell sorting; For imaging flow cytometry, cell debris were gated out and the focused single cells are identified using the IDEAS®6.2 software. Gradient RMS (Root Mean Square) was firstly used to find the focused cells. The Gradient RMS is useful for the selection of focused images by measuring large changes of pixel values in the image and is computed using the average gradient of a pixel normalized for variations in intensity levels. Cells with Gradient RMS value between 40-100 were included for further analysis.

☒ Tick this box to confirm that a figure exemplifying the gating strategy is provided in the Supplementary Information.